

Article

Buckling Resistance and Its Effect on the Gas Barrier of Composite Coating Layers Based on Polyvinyl Alcohol and Montmorillonite

Nur Hanani Zainal Abedin ^{1,2,3,*}, Stefan Schiessl ^{3,4,*} and Horst-Christian Langowski ^{3,4}

¹ Department of Food Technology, Faculty of Food Science and Technology, Universiti Putra Malaysia (UPM), Serdang 43400, Malaysia

² Halal Products Research Institute, Universiti Putra Malaysia (UPM), Serdang 43400, Malaysia

³ Fraunhofer Institute for Process Engineering and Packaging IVV, 85354 Freising, Germany

⁴ TUM School of Life Sciences, Technical University of Munich, 85354 Freising, Germany

* Correspondence: hanani@upm.edu.my (N.H.Z.A.); stefan.schiessl@ivv.fraunhofer.de (S.S.)

† These authors contributed equally to this work.

Abstract: In addition to the mechanical properties and barrier performance, one of the key properties of flexible films used in food packaging is the resistance of their gas barrier layer to buckling and bending. Testing the gas barrier before and after mechanical stress is time-consuming and resource-intensive, but important to assure a certain gas barrier during the whole life time of the package until food consumption. The aim of this study was, on the one hand, to identify the most significant influencing factors of a composite lacquer formulation and coating on its buckling resistance and, on the other hand, to show a fast and efficient method to identify defects occurring during buckling. The influence of mechanical stress was simulated via Gelbo-Flex treatment, and the samples were examined and evaluated before and after using light microscopy. The evaluation was verified with scanning electron microscopy (SEM) and helium barrier measurement. Polyethylene terephthalate (PET) and polyethylene (PE) films were coated with composite barrier lacquers made of polyvinyl alcohol (PVA) and montmorillonite (MMT) and the wet coating layer thickness (20, 40, 80, and 130 μm) and the composition of the coating were changed. It was found that thin coatings are more resistant to buckling than thick coatings. It was also shown that a higher proportion of MMT in the coating layer leads to a better gas barrier, but poorer buckling resistance. Additionally, it was found that soft PE films are already subjected to high stresses during the coating process, which means that barrier coatings do not build up ideally. However, the barrier-coated soft film withstood mechanical stress better and lost less barrier by a lower factor than the counterpart on the basis of PET. To conclude, the evaluation of the buckling resistance with microscopy offers an efficient method during lacquer development; however, the final decision on the right lacquer composition is dependent on many factors.



Citation: Zainal Abedin, N.H.; Schiessl, S.; Langowski, H.-C. Buckling Resistance and Its Effect on the Gas Barrier of Composite Coating Layers Based on Polyvinyl Alcohol and Montmorillonite. *Coatings* **2024**, *14*, 1578. <https://doi.org/10.3390/coatings14121578>

Academic Editor: Elena Torrieri

Received: 24 October 2024

Revised: 9 December 2024

Accepted: 16 December 2024

Published: 17 December 2024

Keywords: permeability; food packaging; Gelbo-Flex; composite barrier coating; buckling resistance



Copyright: © 2024 by the authors. Licensee MDPI, Basel, Switzerland. This article is an open access article distributed under the terms and conditions of the Creative Commons Attribution (CC BY) license (<https://creativecommons.org/licenses/by/4.0/>).

1. Introduction

Food packaging is an essential step during food processing to ensure the safety and quality of food from farm to fork. Prolonged food shelf-life helps to reduce food waste, lessen the cost of production and carbon footprint, and eliminate energy consumption [1]. For this, materials with high barriers to moisture and gases are preferable to avoid fungal contamination [2], oxidation [3], or unwanted texture changes [4]. Therefore, plastic consumption for food applications is still in demand due to the benefits of these materials offered such as their light weight, durability, and low price. This is supported by Statista Research Department [5], wherein global plastic production is shown to have increased and is expected to increase at least until 2027 [6].

Polyethylene terephthalate (PET) and polyethylene (PE) are conventional polymers widely used as packaging materials due to their excellent properties. PET is lightweight, colorless, transparent (in an amorphous state), translucent (in a semi-crystalline state), and inert against many relevant substances to a rather high degree [7]. Additionally, PET has a high strength-to-weight ratio, making it more versatile for wide applications. It has good chemical and physical stability, which makes it the most promising packaging material for drinking water [8,9]. Meanwhile, PE is frequently used due to its excellent water vapor barrier properties and good processability [10,11]. It possesses a broad variation of crystalline structures based on density and chain branching. Owing to this, it is commonly available in two forms: high-density polyethylene (PE-HD) and low-density polyethylene (PE-LD) [11]. Both materials are recyclable, promoting their utilization as sustainable resources, but are nevertheless based on fossil fuels [12]. Therefore, there is a demand in industry to replace petrochemical-based plastics with eco-friendly biodegradable biopolymers, e.g., like polylactic acid (PLA) [13]. PLA is the most employed bio-based material in food packaging because of its similar processing methods and very good mechanical and barrier properties comparable to conventional polymers like polystyrene (PS) and PET [14].

Due to the demand for these materials for broad food packaging applications, there is an urgent need to enhance their barrier properties, particularly towards moisture, oxygen, and volatile odor molecules. Since the intrinsic water vapor barrier of PET and especially PE is high, a common way is to improve the oxygen barrier is by using a coating with polyvinyl alcohol (PVA) [15,16]. PVA is a transparent, flexible, and non-toxic synthetic polymer with resistance to most chemicals. In some variants, it is a biodegradable polymer [17–19]. PVA has also been approved as food contact material by the US Food and Drug Administration (FDA) [20]. Owing to these properties, it is suitable for food packaging applications. The oxygen barrier of PVA coating layers can even be improved by the integration of silicate platelets [21–26]. The combination of a non-polar polymer film and a polar PVA-based coating comprises a polymer film with a barrier against moisture and oxygen.

During transportation, handling, storage, film processing, and usage, the polymer films are exposed to deformation, folding, buckling, and bending. The barrier properties of the films are sensitive to such mechanical stresses, which has a long-term effect on the shelf life of the packaged food. As an overall rule, the higher the barrier of a coating layer, the more rigid the coating layer [27]. Standard oxygen permeability measurement is time-consuming and requires tedious steps [28]. The packaging industry is therefore demanding for a standard, fast, and simple test procedure to determine the influence of the mechanical stresses on the permeability of these polymer materials.

Within this study, a less elastic PET film and an elastic PE film were coated with gas barrier lacquers based on PVA and montmorillonite (MMT). The coating layers were varied in thickness and composition, that is, in terms of the mixing ratio of PVA and MMT. Afterward, the coating surfaces were examined with light and scanning electron microscopy (SEM) and the films were characterized regarding their helium barrier. In the next step, the coated films were exposed to Gelbo-Flex (GF) treatment. This treatment simulates the mechanical stresses that occur during production, including bending, stretching, and folding during the roll-to-roll process from film to pouch, as well as the buckling and crushing that occurs during packaging, shipping, and transport from production to the market and from the market to the end user. After the GF treatment, the films were again characterized using the same analytics to identify which coating layer was more resistant to mechanical stresses. A known disadvantage of the GF treatment is that the kinks, crinkles, and cracks created in the film or coating are random from sample to sample and the test is therefore not considered reproducible [29]. For this reason, a controlled buckling of the coated films with a defined weight was carried out as part of this study and the barrier was measured before and after this defined buckling. In this way, results were obtained after defined buckling and after the GF treatment, which is standard in the industry. The method of optical microscopy we used is a fast and easy method for making a pre-selection which modification in terms of thickness and composition of the lacquer helps to improve

with respect to resistance against bending, folding, and buckling. SEM images and helium barrier measurements were used to confirm the learnings from optical microscopy; these are still faster than typically used oxygen and water vapor measurements. Additionally, an ink test is introduced that was adopted from the field of non-destructive testing that allows for evaluating the influence of the number of GF cycles on the quality of a coating layer with the chosen optical method.

2. Materials and Methods

2.1. Materials

Polyvinyl alcohol (PVA) was obtained as Exceval AQ-4104 from Kuraray (Frankfurt, Germany) with a molecular weight of $32,000 \frac{\text{g}}{\text{mol}}$. Platelet-shaped silicate particles and montmorillonite (MMT) were provided as CLOISITE Na⁺ from BYK Additives and Instruments (Wesel, Germany). The polyethylene terephthalate (PET) film Hostaphan™ RN23 was purchased from Mitsubishi Polyester Film (Wiesbaden, Germany). Polyethylene (PE) film was purchased from Syfan (Kibbutz Saad, Israel). The polylactic acid (PLA) film used was NATIVIA® from Taghleef Industries (Holzhausen an der Haide, Germany). All control films, PET, PE, and PLA, were transparent and provided a thickness of 23 µm.

2.1.1. Lacquer Preparation

As reference coating, one type of PVA lacquer was produced with a solid content of 8 wt% from the PVA granules without further additives. For this purpose, the PVA was mixed with water in a closed beaker at room temperature for 30 min, followed by a heating step to 90 °C and a holding time of 60 min under constant stirring. When the PVA granules showed complete dissolution, the lacquer was cooled down to room temperature. To produce the composite barrier lacquers (CBLs), the MMT dispersion in water was prepared firstly via a ball milling step according to Schiessl et al. [25] with a solid content of 5 wt%. Afterward, the PVA granules were added to the MMT dispersion in a way that the total solid content, meaning PVA and MMT together, was 8 wt%. The dissolving of the PVA granules in the MMT dispersion was carried out as described for pure PVA. The mixing ratio of PVA to MMT was adjusted to be 2:1 and 1:1 in weight with the numbers in the brackets indicating the mixing ratio. The lacquers were labeled with PVA(1:0), CBL(2:1), and CBL(1:1).

2.1.2. Sheet Coating

Before coating, the polymer sheets were pretreated via corona discharge with a dose of $2.9 \frac{\text{kJ}}{\text{m}^2}$ for PE and with a dose of $2.0 \frac{\text{kJ}}{\text{m}^2}$ for PET applied with a table corona unit from Tigres (Marschacht, Germany). The surface energy was measured to be higher than $44 \frac{\text{mN}}{\text{m}}$ by means of test inks (Teststifte PINK, arcotest, Mönshheim, Germany, according to DIN ISO 8296 [30]). Afterward, the lacquers were coated on the sheets with a lab-coating unit CUF 5 (Sumet Messtechnik, Denklingen, Germany) with the k-bar coating technique. Directly after coating, the sheets moved in a convection dryer and the coating layer was dried for 3 min at 60 °C.

The first investigation topic was to determine the effect of the coating thickness on the buckling resistance. Therefore, the same lacquer (CBL(1:1)) was coated with a varying wet layer thickness of 20, 40, 80, and 130 µm. These thicknesses were chosen because they result in dry layer thicknesses from 1 to 10 µm, which is the typical range for barrier lacquer and other functional layers in food industry [31]. The samples were labeled accordingly with the control film (PET or PE), the lacquer, and the wet coating layer thickness, leading to PE | CBL(1:1)-20, for example.

The second investigation topic was to determine the effect of the mixing ratio of polymer material (PVA) and silicate particles (MMT) on the buckling resistance. Therefore, the wet coating layer thickness was kept constant (40 µm) and the lacquer composition was varied. The lacquers PVA(1:0), CBL(2:1), and CBL(1:1) were coated with the same total

solid content of 8 wt%. The samples were labeled similarly, leading to PE|PVA(1:0)-40, for example.

2.2. Methods

2.2.1. Thickness Measurement

The thicknesses of the uncoated and coated control films were measured using a precision thickness gauge (Hanatek FT3 from Rhopoint Instruments, Beyhill on Sea, UK). The resolution was 0.1 μm , the thickness was measured at five random spots on the coated sample, and an average value was reported.

2.2.2. Tensile Test

To determine the tensile strength, the elongation at break, and the Young's Modulus according to DIN EN ISO 527-3 [32], an electromechanical universal testing machine from ZwickRoell (Ulm, Germany) with type Z005 from the Allround Line was used. The traverse velocity was set to 100 $\frac{\text{mm}}{\text{min}}$ and the free clamping length was 50 mm. A fivefold measurement was performed for each sample.

2.2.3. Stereo Microscopy

The stereo microscopy analysis was conducted using a LEICA MZ16 microscope attached to a LEICA DFC320 camera (Wetzlar, Germany) to obtain images of samples using LAS (Leica Application Suite) v4.0 with magnifications of 20 and 40 times. The setup of the stereo microscope allows more detailed information about the surface morphology, but is limited in magnification [33].

2.2.4. Differential Interference Contrast Microscopy

The differential interference contrast (DIC) microscopy was run by a Leitz Diaplan microscope and LEICA DFC295 camera (Wetzlar, Germany) with the software LAS v4.0. The same samples used for stereo microscopy were also used for this analysis. The DIC microscope operates with illumination using polarized white light and reacts to differences in the refractive index or thickness of light-transmitting objects. Stress-induced changes in the refractive index were also detected. These differences lead to a phase shift in the observation light, which generates different colors through interference [34].

2.2.5. Scanning Electron Microscopy

The scanning electron microscopy (SEM) images were captured using a JSM-7200F from JEOL (Akishima, Japan). Before the analysis, samples were sputtered with a gold layer using a Hummer JR (Technics, Alexandria VA, USA). The images of the coating layers on the control films were captured with magnifications of 100 and 1000.

The cross-sections were prepared by Ar^+ beam milling with a cross-section polisher (JEOL). The coated film was adhered between two conductive copper tapes with a conductive adhesive to improve the image quality. The images were captured with a magnification of 10,000.

2.2.6. Defined Buckling

Figure 1 shows the process of defined buckling of the coated films. The films were folded in a way that the coated side was inside. The buckling was performed by rolling a steel cylinder with a defined weight of 1.98 kg two times over the edge. The film was turned by 90° and the steps were repeated, ending up with two kinks building a cross centered in the middle of the sample used for permeability test.

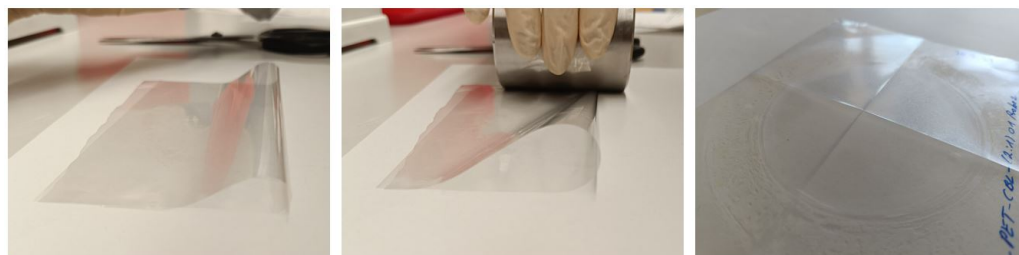


Figure 1. Defined buckling of coated film; the film is folded in a way that the coated side is touching itself (**left**); the film is buckled with a steel cylinder (**middle**); the film is buckled two times with a turning angle of 90° (**right**).

2.2.7. Gelbo-Flex Treatment

Gelbo-Flex (GF) treatment was conducted according to ASTM F392 [35] by mounting the control films and coated films as A4 sheets on the Gelbo-Flex Tester (KFT Brugger München, Germany) and treating them with 3 and 10 cycles of back and forth twisting of 440°.

2.2.8. Helium Permeability Test

The helium permeability coefficients P_{He} were determined using the manometric measurement principle according to DIN 53380-2 [36] at a temperature of 23 °C and a relative humidity of 0%RH. The test device was a GDPE from Brugger Feinmechanik (Munich, Germany). A twofold measurement was performed for each sample and the values were reported with standard deviation. With the helium permeance Q_s of the uncoated substrates PE and PET and the total permeance of the coated films Q_t , being the measured values, the permeance of the coating layer Q_c was calculated according to Equation (1).

$$Q_c = \frac{Q_s \cdot Q_t}{Q_s + Q_t} \quad (1)$$

Normalizing the permeance to a specific layer thickness, in this study, 1 μm leads to the permeability coefficient of the coating layer with the unit $\frac{\text{cm}^3 \text{ (STP)} \mu\text{m}}{\text{m}^2 \text{ d bar}}$ [37].

2.2.9. Ink Test

The application of this test was motivated by a commonly used method in the area of non-destructive testing, penetrant testing or dye penetrant inspection [38,39]. The test was performed by using a marker, Faber-Castell multimark permanent (Stein, Germany), to observe the penetration behavior of the marker's ink in inhomogeneities of the buckled films after GF treatment. The method is simple, whereby the leaking of ink through the crinkles or cracks emphasizes a defect or delamination of the coating layer visually. During this analysis, the flexed films coated with different barrier lacquer formulations were marked with blue marker ink. After 10 min, each sample was investigated with DIC microscopy with a magnification of 40 times to see the penetration behavior.

3. Results and Discussion

3.1. Tensile Test

Table 1 lists the results of the tensile tests of the uncoated control films: PET, PE, and PLA. It is known that PET is a stiffer material than PE [40], which was also reflected in the higher values for the Young's Modulus (4100 MPa for PET and 141 MPa for PE) and tensile strength (252 MPa for PET and 85 MPa for PE) of the films used. Consequently, the PET film (105%) comprised a lower elongation at break than the PE film (132%). The mechanical properties of the control films in addition to the adhesion of the lacquer to these control films are the decisive characteristic when it comes to how the coated film behaves during GF treatment [41].

Table 1. Results of the tensile test of the polyethylene terephthalate (PET), the polyethylene (PE), and the polylactic acid (PLA) control films, each with a thickness of 23 μm .

Polymer Film	Young's Modulus MPa	Tensile Strength MPa	Elongation at Break %
PET-control	$4.10 \times 10^3 \pm 148$	252 ± 9.03	105 ± 3.20
PE-control	141 ± 28.8	84.5 ± 3.02	132 ± 3.50
PLA-control	$3.09 \times 10^3 \pm 123$	105 ± 2.38	38.6 ± 4.70

The PLA control film was an outlier in this study. Even when providing a similar thickness as PET and PE, the uncoated version of the PLA film already broke during one cycle of GF treatment. The very low value for the elongation at break (38.6%) in combination with its rigidity (3090 MPa) was the reason why PLA was not suitable as a control film for the planned investigation.

3.2. Effect of Coating Layer Thickness

3.2.1. Dry Coating Layer Thicknesses

The thickness values of coated PET and PE films are listed in Table 2. Applying 20 μm of CBL(1:1) lacquer with a total solid content of 8 wt% on both PET and PE film only led to a dry layer thickness of 0.8 and 1.7 μm , respectively. A wet coating layer thickness of 40 μm led to 2.7 and 4.1 μm , a wet coating layer thickness of 80 μm led to 5.9 and 7.2 μm , and a wet coating layer thickness of 130 μm led to 7.3 and 9.3 μm , respectively. As expected, the dry layer thickness increased with increasing wet layer thickness for both substrates. However, within the substrates, the dry layer thicknesses differed, with a consistently thicker coating layer on PE compared to PET. The k-bar coating technique used is self-metered; i.e., the coating thickness depends on the total solid content, the viscosity, the flow behavior, and the interaction of the lacquer and the control film in addition to the wet film thickness [42]. As an overall rule during a self-metered coating process, the theoretical coating thickness is always higher than the actual achieved one since the lacquer is not entirely transferred on the substrate, but there are some losses. The goal to investigate the effect of the dry coating layer thickness on the buckling behavior of the two substrate films could be tackled since four distinctly different coating layers were produced.

Table 2. Thickness values and helium permeability coefficients of CBL(1:1) coating layers applied with different wet coating layer thicknesses of 20, 40, 80, and 130 μm on polyethylene terephthalate (PET) and polyethylene (PE) films.

Sample Code	Thickness μm	Permeability Coefficient $\frac{\text{cm}^3(\text{STP})\mu\text{m}}{\text{m}^2\text{d bar}}$	Sample Code	Thickness μm	Permeability Coefficient $\frac{\text{cm}^3(\text{STP})\mu\text{m}}{\text{m}^2\text{d bar}}$
PET-control	23 ± 0.2	$4.2 \times 10^4 \pm 8.9 \times 10^2$	PE-control	23 ± 0.3	$3.3 \times 10^5 \pm 3.8 \times 10^3$
PET CBL(1:1)-20	0.8 ± 0.2	$4.1 \times 10^1 \pm 3.0$	PE CBL(1:1)-20	1.7 ± 0.3	$6.0 \times 10^3 \pm 1.6 \times 10^2$
PET CBL(1:1)-40	2.7 ± 0.4	$3.9 \times 10^1 \pm 2.1$	PE CBL(1:1)-40	4.1 ± 0.6	$6.4 \times 10^3 \pm 1.7 \times 10^2$
PET CBL(1:1)-80	5.9 ± 0.3	$3.8 \times 10^1 \pm 2.9$	PE CBL(1:1)-80	7.2 ± 0.5	$6.7 \times 10^3 \pm 1.3 \times 10^2$
PET CBL(1:1)-130	7.3 ± 0.5	$5.5 \times 10^1 \pm 5.0$	PE CBL(1:1)-130	9.3 ± 0.6	$8.5 \times 10^3 \pm 2.5 \times 10^2$

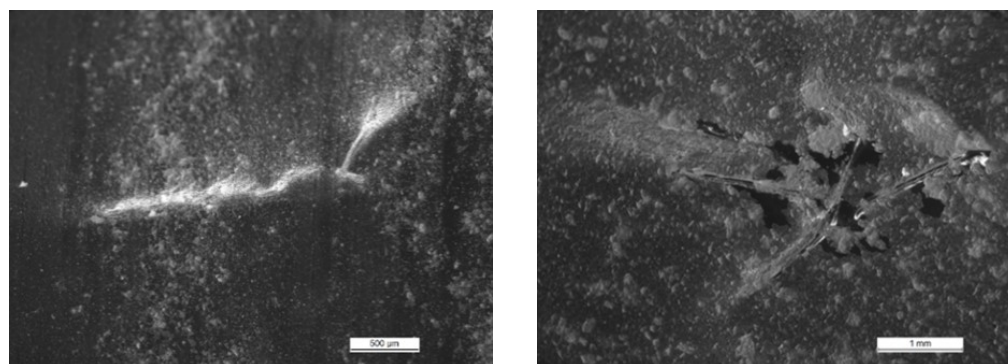
3.2.2. Light Microscopy with Stereo and Differential Interference Contrast Microscope

Within the two substrates, the surface of the PE film is distinctly rougher than the surface of the PET film. This property could be seen best on the images taken with the stereo microscope, which, due to its mode of operation, provides more information on the surface structure (Figure A1). Yan et al. [43] found the same for the two materials. The reason for this lies in the crystalline structure. In the case of PET, the alternating terephthalate

and ethylene glycol units lead to a highly regular and rigid molecular structure, leading to a smooth surface. In comparison to PET, PE comprises a more random and flexible molecular structure due to the presence of branching. The level of crystallinity in PE is lower compared to PET, meaning the polymer chains are not as tightly packed. This more amorphous structure makes PE films softer and less smooth compared to PET.

The difference in roughness between the two substrates is no longer recognizable after coating with the composite lacquer CBL(1:1) and the other lacquer formulations described later in Section 3.3. The roughness of the dried composite coating layer is thus independent of the substrate. The influence of the applied layer thickness is only marginal. For both substrates, the roughness tends to increase slightly with increasing layer thickness. The roughness is caused by agglomerates of MMT in the lacquer that were not sheared off during the manufacturing process or were newly formed during coating. If a thin wet layer is applied, it is more likely that larger agglomerates are pushed forward by the k-bar and thus do not end up in the dry layer. On the other hand, there is the drawback for thin wet coating layers that the probability increases for smaller agglomerates, potentially becoming stuck between the k-bar and the substrate, leaving a stripe in the coating layer.

Figure 2 shows images generated with the stereo microscope of the PET film coated with 0.8 and 7.3 μm of the CBL(1:1) after GF treatment. After the treatment, PET | CBL(1:1)-20 and PET | CBL(1:1)-40 showed crinkles and stretch marks but no holes. The images taken with the DIC microscopy gave additional information (Figure A3). The tiny lines not only appeared on the coating surface, but also in the coating layer, indicated by the rainbow colored area interfering with the polarized light from the DIC microscope in and around the stretch marks [44]. An increase of the coating layer thickness to 5.9 and 7.3 μm led not only to crinkles and stretch marks, but to holes in the coating layer. These holes could be best observed with the stereo microscope. The DIC microscopy again shows the mechanical tension created by the GF treatment in the coating layer but also in the substrate itself since the rainbow colored area was observed directly in the center of the hole.



(a) PET | CBL(1:1)-20 after 10 cycles GF

(b) PET | CBL(1:1)-130 after 10 cycles GF

Figure 2. Stereo microscope images of the 0.8 μm thick (left) and the 7.3 μm thick (right) coating layer of CBL(1:1) on the PET film after ten cycles of Gelbo-Flex treatment. The whole series of images with all applied coating layer thicknesses of CBL(1:1) on PET before and after Gelbo-Flex treatment is shown in Figure A2 for stereo microscopy and in Figure A3 for DIC microscopy.

Figure 3 shows images generated with the stereo microscope of the coated PE film with a coating layer thickness of 1.7 μm before and after GF treatment. In comparison to the similarly coated PET film, the thin CBL(1:1) coating on the PE film showed no optical change (no crinkles and stretch marks) due to the GF treatment. The more elastic appearance of PE, indicated by the lower Young's Modulus and higher elongation at break, shown in Section 3.1, led to a better force distribution in the coating layer during the mechanical stress of the GF treatment. The images generated with DIC microscopy of the coated PE films after GF treatment showed no light refraction of the polarized light, as was the case for the PET samples (Figure A5). It seems that the tensions were created mainly in

the control film, not in the coating layer. An increase of the coating layer thickness from 4.1 to 7.2 μm on PE also led to holes in the coating layer as it did for similarly coated PET samples. The rigidity of the CBL(1:1) coating layer itself was one reason for the visible delamination in the form of holes. Additionally, it is known that the adhesion of PVA-based lacquers is better on PET than on PE [45] and a better adhesion of the coating layer to the control film leads to better performance during the GF treatment [46].

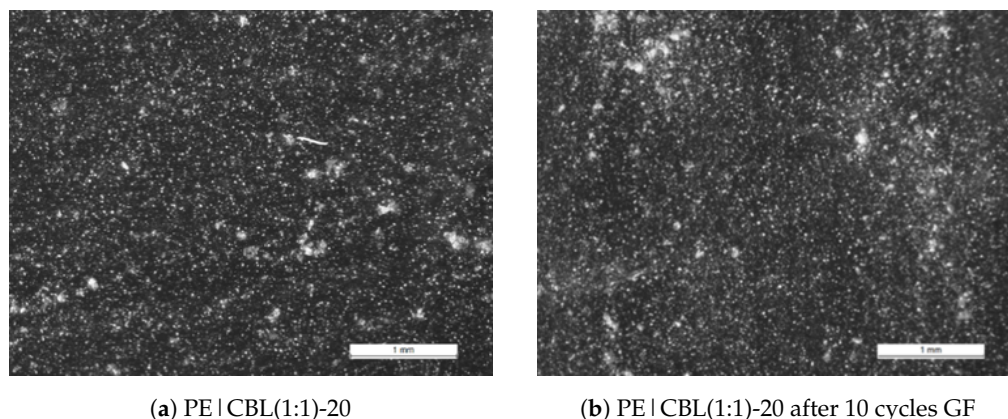


Figure 3. Stereo microscope images of the 1.7 μm thick CBL(1:1) coating layer on the PE film before (left) and after ten cycles of Gelbo-Flex treatment (right). The whole series of images with all applied coating layer thicknesses of CBL(1:1) on PE before and after Gelbo-Flex treatment is shown in Figure A4 for stereo microscope and in Figure A5 for the DIC microscope.

This means that the ideal thickness of a CBL (1:1) coating is crucial to ensure robust structures of coated films combined with sufficient barrier properties. In this case, a lower coating thickness is preferable, offering benefits to the plastics and food industries in terms of reduced material usage, lower costs, and lighter products.

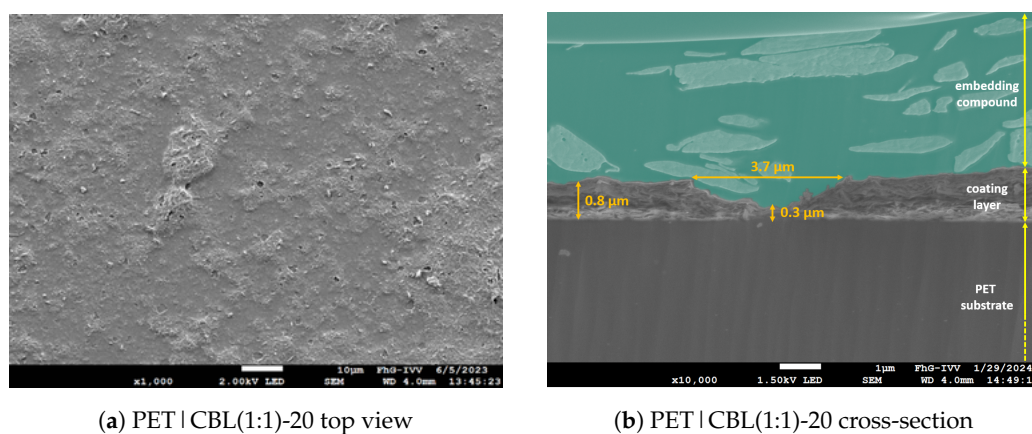
3.2.3. Scanning Electron Microscopy

In principle, the SEM images confirm the results of light microscopy (Figures A6 and A7). Nevertheless, there are decisive advantages when observing the material with SEM, both at a low magnification of 100 and at a higher magnification of 1000.

In SEM images with a magnification of 100 (Figures A6 and A7), the surface is represented as sharper and the imaging of backscattered electrons makes it easier to detect cracks. When evaluating the light microscopy images, there was no difference in the thick coating of CBL(1:1) on PET and PE. However, the SEM images show that the thick coating layers on PE already showed small cracks and inhomogeneities before the GF treatment, which was not the case with PET. Two reasons were identified for why coating on PE was more challenging with the lacquer used. First, the surface tension of PE was lower than for PET even after corona pre-treatment and the wetting and adhesion behavior of the aqueous layer on PE might be different than on PET [47]. Second, the films were mechanically stressed during the k-bar coating process. The k-bar was pressed with a force of 20 N on the film and the film was heated up to 60 $^{\circ}\text{C}$ for 3 min. This mechanical stress affected the PE film more than the rigid and temperature-stable PET film. During the coating or drying, the PE film might be stretched and relaxed more than PET, leading to cracks before GF treatment.

When the cracks and holes become bigger and their number is increasing after GF treatment, they can also be identified also light microscopy. The SEM images after GF treatment confirm the findings made with light microscopy. It is therefore concluded that the influence of the GF treatment on the coating layer can be identified quickly with light microscopy and the elaborated sample preparation for SEM is not necessary. For a detailed investigation of the surface, however, the SEM images with a magnification of 100 are useful since they provide additional information.

An increase of the SEM magnification to $1000\times$ led to another observation shown in Figure 4. The dried surface of the CBL lacquer featured in an increasing number of craters and holes compared to increasing wet coating layer thickness. These craters and holes appeared during the drying process for the following reasons. The CBL layers contain microbubbles of air that are incorporated in the wet coating layer. During the drying process, the thermal expansion of these air bubbles is larger by a factor of 1000 than the thermal expansion of the dried lacquer. Therefore, the craters and holes come from bursting air bubbles during drying [48]. The thinner the wet coating layer is, the higher the probability for these bubbles to be sheared off or pushed along the k-bar bead. Hence, there are more air bubbles incorporated in the thick wet coating layers and consecutively more craters and holes in the dried CBL layer for thicker coating layers. The cross-section image of such a crater shows that the substrate is still completely coated, meaning that the air bubble is not causing a hole through the whole coating layer, but the coating thickness is distinctly decreased at the bottom of those craters, potentially leading to a decrease in gas barrier performance. This phenomenon was only observed with the higher magnification that was available during SEM investigation and would not have been recognized only with light microscopy.



(a) PET | CBL(1:1)-20 top view

(b) PET | CBL(1:1)-20 cross-section

Figure 4. Scanning electron microscopy image of the surface of the dried CBL(1:1) lacquer coated on PET (**left**) with a wet layer thickness of $20\ \mu\text{m}$ with a magnification of 1000. (**Right**) Cross-section SEM image of the same sample, including a crater induced by an air bubble.

3.2.4. Helium Barrier

Figure 5A shows the helium permeance of the uncoated and coated PET film. The uncoated PET film exhibits a He permeance of $1816\ \frac{\text{cm}^3(\text{STP})}{\text{m}^2\ \text{d}\ \text{bar}}$. This value decreases to $52\ \frac{\text{cm}^3(\text{STP})}{\text{m}^2\ \text{d}\ \text{bar}}$ when the PET film is coated with the thinnest layer of CBL(1:1) having a dry thickness of $0.8\ \mu\text{m}$. An increase in the coating layer thickness to $5.9\ \mu\text{m}$ decreases the helium permeance to $6.5\ \frac{\text{cm}^3(\text{STP})}{\text{m}^2\ \text{d}\ \text{bar}}$. Further increases in the layer thickness did not lead to further barrier improvements, probably because the amount of inhomogeneities like the craters shown in Section 3.2.3 reached a critical level for the layer thickness of $7.3\ \mu\text{m}$. Conversion to the permeability coefficient confirms the inversely proportional dependence of the permeance on the layer thickness (Table 2). A constant permeability coefficient of 38 to $41\ \frac{\text{cm}^3(\text{STP})\ \mu\text{m}}{\text{m}^2\ \text{d}\ \text{bar}}$ is obtained for coating thicknesses from 0.8 to $5.9\ \mu\text{m}$. This value is in the same range as a previously reported value on PET for the same lacquer [26]. Consequently, the permeability coefficient obtained for a $7.3\ \mu\text{m}$ thick layer does not match these and, for the reasons given, is $55\ \frac{\text{cm}^3(\text{STP})\ \mu\text{m}}{\text{m}^2\ \text{d}\ \text{bar}}$.

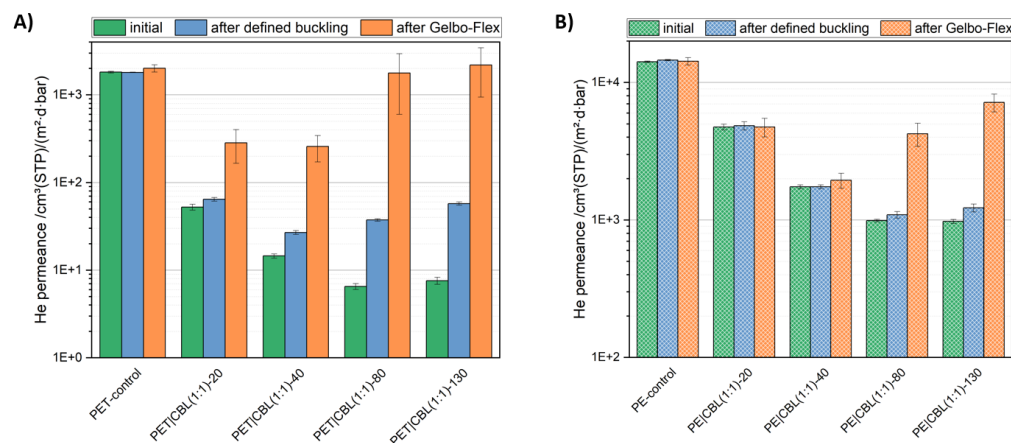


Figure 5. Helium permeance of the PET (A) and PE (B) control films and the films coated with CBL(1:1) in different layer thicknesses. The measurement was performed initially, after defined buckling, and after 10 cycles of Gelbo-Flex treatment. The respective permeability coefficients of the coating layers normalized to a layer thickness of 1 μm are shown in Figure A9.

After defined buckling, the permeance increased for the coated films, while the buckling had no influence on the permeance of the control film. The increase in permeance, which is synonymous with a deterioration of the gas barrier, is more pronounced the thicker the coating is. While the permeance only changes by 22% from 52 to 64 $\frac{\text{cm}^3(\text{STP})}{\text{m}^2 \text{ d bar}}$ for the thin coating (0.8 μm), the permeance changes by more than 4.5 times from 6.5 to 37 $\frac{\text{cm}^3(\text{STP})}{\text{m}^2 \text{ d bar}}$ for the thicker coating (5.9 μm).

The permeance of the control film was not affected by the GF treatment, but the permeance of the coated films. Since the GF treatment subjects the films to greater mechanical stress than the defined buckling, this was to be expected. The thin and medium-thick CBL(1:1) coating exhibited a permeance of 284 and 258 $\frac{\text{cm}^3(\text{STP})}{\text{m}^2 \text{ d bar}}$, respectively, which is at least distinctly below the value for the uncoated film. The GF treatment of the two thicker coatings led to a situation where the effect of the coating layer was gone. This was expected due to the macro holes and the delamination of the coating layer seen in the optical investigation.

Figure 5B shows the helium permeance of the uncoated and coated PE film. The permeance of the uncoated PE film is 14.152 $\frac{\text{cm}^3(\text{STP})}{\text{m}^2 \text{ d bar}}$, which was not changed by the mechanical treatment via buckling or GF. As in the coating with CBL(1:1) on PET, the He permeance decreases with increasing coating layer thickness. However, the He permeability coefficients of the coating layers are by two orders of magnitude higher for PE films compared to the PET films. For example, the CBL(1:1)-40 coating exhibited a value of 39 $\frac{\text{cm}^3(\text{STP}) \mu\text{m}}{\text{m}^2 \text{ d bar}}$ on PET but 6366 $\frac{\text{cm}^3(\text{STP}) \mu\text{m}}{\text{m}^2 \text{ d bar}}$ on PE. The reason for this is that even if the value for the gas barrier is mainly determined by the coating layer and not the substrate, the coating performs differently depending on the substrate. Li et al. [41], for example, showed that when PP and PA films are coated with cellulose nanocrystals, the permeability coefficient of the coating is higher by a factor of 127 (also two orders of magnitude) for PP than for PA. There are many reasons for this. The permeability depends on the roughness of the film, the interaction of the coating with the surface, the adhesion of the coating to the surface, the crystallization behavior, and the flow behavior of the lacquer on the film. In addition, it was shown in Section 3.1 that the PE film has a higher elongation and a lower stiffness compared to the PET film. During the coating and drying process and after the handling of the coated films, the coating layer is exposed to mechanical stresses that are better resisted by the PET film. This is, for example, indicated by the SEM images of the PE coated with 7.2 and 9.3 μm CBL(1:1), where already the non-treated films showed some defects, which was not the case for similarly coated PET.

A comparison of the performance of the CBL(1:1) coating on PET and PE after mechanical treatment shows the following. The coating layer on the PE film resists the mechanical treatment better due to a lower loss of barrier performance, and after defined buckling, the He permeance is close to the initial values before mechanical treatment for all coating layer thicknesses. This is also true for the treatment with GF for the thin and medium thickness layers. The He permeance only increases significantly after the GF treatment for the thicker coating layers, but does not reach the initial values of the uncoated PE control film. The coating layers on the PE film are therefore more resistant to mechanical treatment. Due to the mechanical properties of PE, which is less rigid than PET, the stresses are distributed more homogeneously across the coating layer, resulting in fewer defects.

Regarding the coating layer thickness, it is concluded that for a coating with CBL(1:1), a thin coating layer is suggested, since it withstands the mechanical stresses better than thicker coating layers independently from the substrate.

3.3. Effect of Fraction of Montmorillonite

3.3.1. Dry Coating Layer Thickness

To investigate the effect of the MMT fraction on the buckling behavior, all lacquers shown in this section were coated with a k-bar giving a wet layer thickness of 40 μm and had a total solid content of 8 wt%. This would theoretically result in the same coating thickness. As shown in Table 3, this was not the case, since the k-bar coating is considered to be self-metered (Section 3.2.1). Applying the PVA(1:0) lacquer led to coating thicknesses of 3.9 and 4.8 μm on PET and PE, respectively. The addition of MMT to a mixing ratio of 2:1 led to layer thicknesses of 3.1 and 4.4 μm on PET and PE. A further increase in MMT content to a mixing ratio of 1:1 finally led to thicknesses of 2.7 and 4.1 μm , respectively. Hence, an increasing amount of MMT led to a slightly decreasing layer thickness. Since the mixing ratio of PVA and MMT is adjusted in weight, but the density of MMT ($2.86 \frac{\text{g}}{\text{cm}^3}$) differs from the density of PVA ($1.32 \frac{\text{g}}{\text{cm}^3}$), this was to be expected. Nevertheless, the differences in final coating layer thicknesses were only marginal compared to Section 3.2, explaining why the findings in this section are related to the difference in the lacquer formulations.

Table 3. Thickness values and helium permeability coefficients of the coating layers with different MMT fractions on polyethylene terephthalate (PET) and polyethylene (PE).

Sample Code	Thickness μm	Permeability Coefficient $\frac{\text{cm}^3(\text{STP})\mu\text{m}}{\text{m}^2\text{dbar}}$	Sample Code	Thickness μm	Permeability Coefficient $\frac{\text{cm}^3(\text{STP})\mu\text{m}}{\text{m}^2\text{dbar}}$
PET PVA(1:0)-40	3.9 \pm 0.2	$1.5 \times 10^3 \pm 4.0 \times 10^1$	PE PVA(1:0)-40	4.8 \pm 0.3	$2.5 \times 10^4 \pm 2.1 \times 10^2$
PET CBL(2:1)-40	3.1 \pm 0.4	$1.7 \times 10^2 \pm 5.9$	PE CBL(2:1)-40	4.4 \pm 0.6	$1.2 \times 10^4 \pm 1.7 \times 10^2$
PET CBL(1:1)-40	2.7 \pm 0.4	$3.9 \times 10^1 \pm 2.1$	PE CBL(1:1)-40	4.1 \pm 0.6	$6.4 \times 10^3 \pm 1.7 \times 10^2$

3.3.2. Light Microscopy with Stereo and Differential Interference Contrast Microscope

Figure 6 shows the effect of the mixing ratio on the morphology of the coating layers on PET after 10 cycles of GF treatment. The PVA(1:0) coating layer showed a small area of tension indicated by the rainbow-colored area coming from the light refraction around the kink. The CBL(1:1) coating layer, on the other side, shows larger areas of mechanical stresses and a higher amount of kinks and crinkles. As expected after the investigation in Section 3.2, no holes were observed for coatings with 40 μm on PET, neither for the most flexible PVA(1:0) nor for the most rigid CBL(1:1). The addition of MMT to PVA increased the stiffness of the coating layer [49]. In this case, increased stiffness or a higher Young's Modulus is accompanied by reduced elongation (ductility), which means that the forces that occur during mechanical stresses are less well distributed, resulting in more tension areas and cracks. This increased stiffness is directly displayed in the DIC microscopy images of the coating layers. With increasing MMT amount, the amount and size of tension

areas in the coating layers on PET increase. The images with the stereo microscope before and after GF treatment show a slight increase in roughness before and after GF treatment, but for identifying tensions in the substrate and the coating layer, DIC microscopy is better suited.

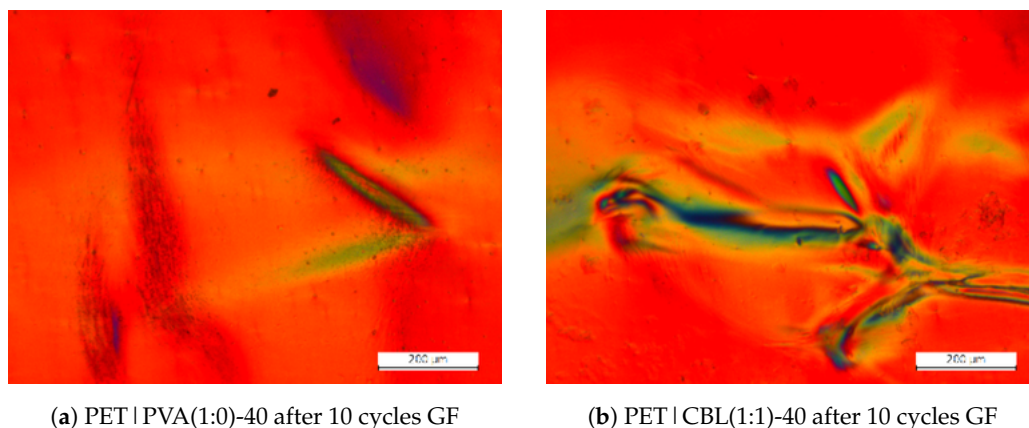


Figure 6. DIC microscope images of the PVA(1:0) and CBL(1:1) coatings on PET after 10 cycles of Gelbo-Flex treatment. The whole series of images with coatings of all formulations on PET before and after Gelbo-Flex treatment is shown in Figure A10 for the stereo microscope and in Figure A11 for the DIC microscope.

The effect of the MMT fraction on the morphology of the coating layers after the GF treatment on PE is shown in Figure 7. Similar to the investigation of different coating thicknesses in Section 3.2, no rainbow-colored tension lines were observed for the coated PE films. However, the increasing amount of black areas with increasing MMT amount in the formulation confirmed the findings for the coating formulation made on PET: the higher the MMT amount, the higher the stiffness of the coating layer, and a higher stiffness in the coating layer leads to less resistance against the GF treatment. The images taken with the stereo microscope showed a delamination behavior of the PVA(1:0) coating layer on PE after GF treatment. The phenomena of the better adhesion of PVA to PET compared to PE was described in Section 3.2.4.

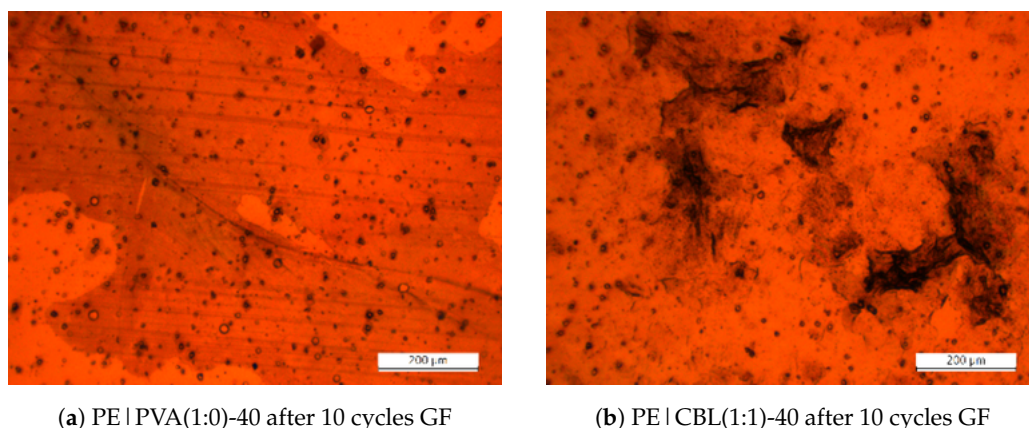


Figure 7. DIC microscope images of the PVA(1:0) and CBL(1:1) coatings on PE after 10 cycles of Gelbo-Flex treatment. The whole series of images with coatings of all formulations on PE before and after Gelbo-Flex treatment is shown in Figure A12 for the stereo microscope and in Figure A13 for the DIC microscope.

3.3.3. Scanning Electron Microscopy

As with our investigations into the influence of layer thickness and into the MMT fraction, the coating surfaces were investigated with SEM (Figures A14 and A15). A magnification of 100 was used to have an overview of a greater area to see crinkles, kinks,

and cracks, which would have been lost without a detailed magnification. The SEM images confirmed the findings from optical microscopy. An addition of MMT to the CBL led to an increased surface roughness. The wet coating layer thickness of 40 μm did not lead to visible cracks or holes in the case of both control films after GF treatment.

Figure A16 shows the PET films coated with the three lacquer formulations, PVA(1:0), CBL(2:1), and CBL(1:1), before GF treatment with a magnification of 1000. Similar to the previous investigation of the coating layer thickness, occurring craters and holes now became visible. It has been shown previously that the viscosity of the lacquers increases with increasing MMT content [50,51]. The increased viscosity led to reduced mobility of the micro air bubbles. The SEM images confirmed this expectation. Whereas the PVA coating layer was quite smooth with only a few inhomogeneities, the number of craters and holes increases with increasing MMT content.

3.3.4. Helium Barrier

Figure 8A shows the helium permeance of the coated PET films with different lacquer formulations. As expected, the barrier performance of the coating layer was improved by the addition of MMT particles [22,25]. The permeability coefficient of the pure PVA coating on PET was $1546 \frac{\text{cm}^3(\text{STP}) \mu\text{m}}{\text{m}^2 \text{ d bar}}$. It decreased to 165 and $39 \frac{\text{cm}^3(\text{STP}) \mu\text{m}}{\text{m}^2 \text{ d bar}}$ for the lacquers CBL(2:1) and CBL(1:1), respectively. This is an improvement factor of 40 for an integration of 50 wt% MMT compared to a pure PVA layer.

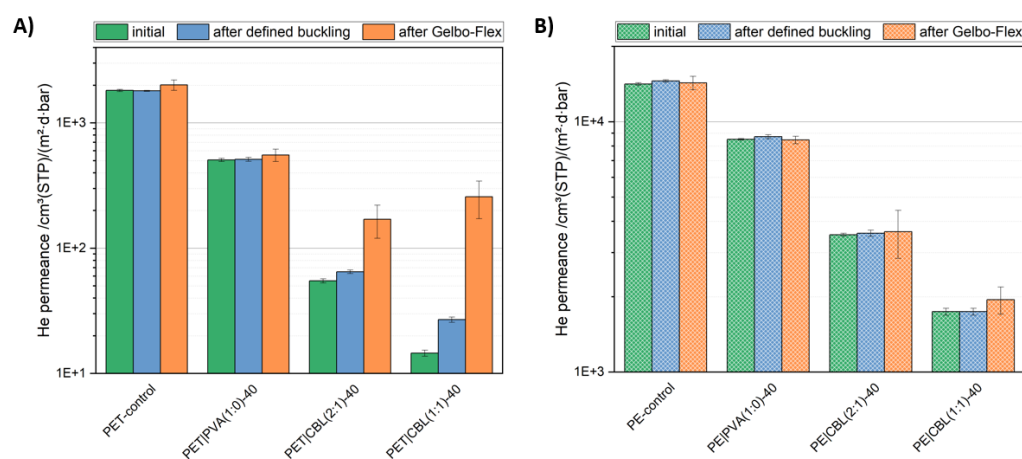


Figure 8. Helium permeance of the PET (A) and PE (B) control films and the films coated with a constant wet layer thickness with lacquers varying in MMT fraction. The measurement was performed initially, after defined buckling, and after 10 cycles of Gelbo-Flex treatment. The respective permeability coefficients of the coating layers normalized to a layer thickness of 1 μm are shown in Figure A17.

After mechanical treatment with defined buckling and GF, the values for the helium permeance changed as expected. The barrier property of the most elastic coating, the pure PVA coating layer, was not affected distinctly by the mechanical treatment. One result which is valid for this coating and for all other coatings and even the control films themselves is that the standard deviation of the GF treated samples was always higher than for the samples that had been defined buckled. This is the main disadvantage of the GF treatment. It leads to strongly deviating individual measurement values, since the mechanical stress from treatment to treatment cannot be reproduced exactly enough. With increasing MMT amount, the coating layer became more sensitive to the mechanical stresses, again with a stronger effect of the GF treatment than the defined buckling. The helium permeance of the PET | CBL(2:1) sample changed from 55 to 65 $\frac{\text{cm}^3(\text{STP})}{\text{m}^2 \text{ d bar}}$ after defined buckling but to 171 $\frac{\text{cm}^3(\text{STP})}{\text{m}^2 \text{ d bar}}$ after 10 cycles of GF treatment. The loss in barrier performance

was even more pronounced for the PET | CBL(1:1) sample where the helium permeance changed from 15 to $258 \frac{\text{cm}^3 (\text{STP})}{\text{m}^2 \text{ d bar}}$ after 10 cycles of GF treatment. Hence, the results from the helium barrier investigation confirm the findings from Sections 3.3.2 and 3.3.3, where CBL(1:1) turned out to be the most rigid coating layer with the most significant changes after GF treatment.

Figure 8B shows the helium permeance of the coated PE films with different lacquer formulations. Similar to PET as substrate, the helium barrier decreases with increasing MMT amount. However, as already mentioned in Section 3.2.4, the permeability coefficients of the coating layer differ distinctly whether they are applied on PET or on PE. On PE, the permeability coefficient of the pure PVA coating layer is $25,522 \frac{\text{cm}^3 (\text{STP}) \mu\text{m}}{\text{m}^2 \text{ d bar}}$ and changes to 12,455 and $6366 \frac{\text{cm}^3 (\text{STP}) \mu\text{m}}{\text{m}^2 \text{ d bar}}$ for lacquers CBL(2:1) and CBL(1:1), respectively.

Comparing the values for the helium permeance after mechanical treatment shows that the barrier performance of the coating layers on PE was distinctly less influenced by the mechanical stresses. The reasons therefor have already been given in Section 3.2.

3.3.5. Ink Test

In typical liquid penetrant testing, the capillary attraction forces the penetrant to enter in the opening of defects [52]. In this analysis, PET and PE control films coated with PVA(1:0) and CBL(2:1) were treated with 3 and 10 cycles GF, respectively. Afterward, the treated samples were marked with the ink and were rested for 10 min. Images taken with the DIC microscope are shown in Figure 9.

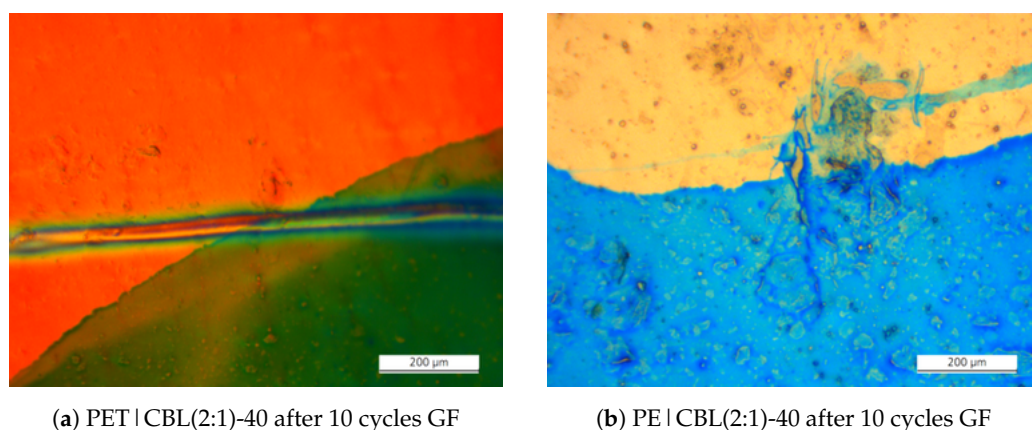


Figure 9. Two samples investigated with the ink test. The ink is the green (left) and blue (right) lines on the bottom of the images and penetrates the cracks induced by the GF treatment. The whole series of images is shown in Figure A18.

The green and blue lines are the ink lines made with a marker. It was observed that the capillary forces that pull the ink into the cracks were stronger for samples treated with 10 cycles of GF than for samples treated only with 3 cycles. It was visible that the blue colored ink was penetrating in the direction of the crack after 10 cycles. This observation was only made with the ink test and not with the previously performed microscope images. Therefore, the ink test is in specific cases a reliable option to investigate crack formation after buckling.

4. Conclusions

This study adds additional knowledge to the topic of the mechanical stress resistance of coated polymer films. PET and PE films were coated with composite barrier lacquers comprising PVA and MMT.

It was found that optical microscopy is suited to investigate the influence of mechanical stresses arising by defined buckling and GF treatment in barrier coating layers. Stereo microscopy turned out to be preferred for identifying holes, delamination, and roughness

of the coating surface. DIC microscopy in combination with polarized light turned out to allow for seeing arising tensions (due to mechanical treatment) in the polymer films and coating layers by areas appearing in rainbow colors due to light refraction. This offered the possibility of seeing defects in coated films even before delamination. Since the examination with the light microscopes worked with transparent PVA, it can be assumed that this examination option can be applied to many lacquer and composite lacquer systems. The main limitation will be the layer thickness of the coatings, because layers that are too thin may not be clearly distinguishable from the substrate, and layers that are too thick or free-standing films will show very large macrodefects after mechanical stress, which may be visible to the naked eye. The SEM images required more time to be prepared and confirmed the findings from the optical microscopy at a magnification of 100. An increase in magnification to 1000 established the possibility of investigating the curing phenomena of microbubbles leading to craters in the dried coating layer. Helium permeability measurement confirmed the expected barrier performance of films after GF treatment.

Firstly, two trends were observed independently of the substrate. On the one hand, the helium permeance decreased with increasing thickness of the composite barrier layer. On the other hand, increasing the MMT content of the composite barrier layer decreased the helium permeance. Secondly, it was found that the permeability coefficients of coating layers varied depending on the substrate. For a similarly applied lacquer, the helium permeability coefficient on PET is two orders of magnitude lower than on PE. For the PVA reference coating, this gave a helium permeability coefficient of $1546 \frac{\text{cm}^3(\text{STP}) \mu\text{m}}{\text{m}^2 \text{ d bar}}$ on PET and $25,522 \frac{\text{cm}^3(\text{STP}) \mu\text{m}}{\text{m}^2 \text{ d bar}}$ on PE. Due to its lower elasticity, the PET film is not as resistant to mechanical treatment as the PE film. For example, for a coating with CBL (1:1), the helium permeability coefficient on PET increased by 1500% after 10 cycles of GF, while the permeability coefficient on PE increased by only 10%. Halving the amount of MMT resulted in only a 191% increase in the permeability coefficient on PET after GF treatment. For a reference coating of pure PVA, the increase in permeability coefficient on PET after GF treatment was only 10%.

Ultimately, a compromise will have to be found for future applications. To achieve the highest possible gas barrier, a thick coating and a high MMT content in the coating layer are desirable. To achieve the highest possible buckling resistance of the coating and thus the packaging, a low MMT content and the thinnest possible coating are advisable. Depending on the product to be packaged and the packaging design, a balance must be struck between these two tendencies in order to find a suitable solution.

Author Contributions: Conceptualization, S.S. and H.-C.L.; methodology, N.H.Z.A. and S.S.; formal analysis, N.H.Z.A., S.S. and H.-C.L.; investigation, N.H.Z.A. and S.S.; data curation, N.H.Z.A.; writing—original draft preparation, N.H.Z.A. and S.S.; writing—review and editing, H.-C.L.; supervision, H.-C.L. All authors have read and agreed to the published version of the manuscript.

Funding: This work received funding from the European Union's Horizon 2020 research and innovation program under grant agreements n°862156 and the FlexFunction2Sustain project.

Institutional Review Board Statement: Not applicable.

Informed Consent Statement: Not applicable.

Data Availability Statement: The data presented in this study are available on request from the corresponding author(s). The data are not publicly available for reasons of confidentiality in the aforementioned EU projects; see the "Funding" section.

Acknowledgments: The authors would like to thank Sandra Diener for executing the SEM analysis.

Conflicts of Interest: The authors declare no conflicts of interest.

Appendix A. Effect of Coating Layer Thickness

Appendix A.1. Surface Images of Uncoated Control Films

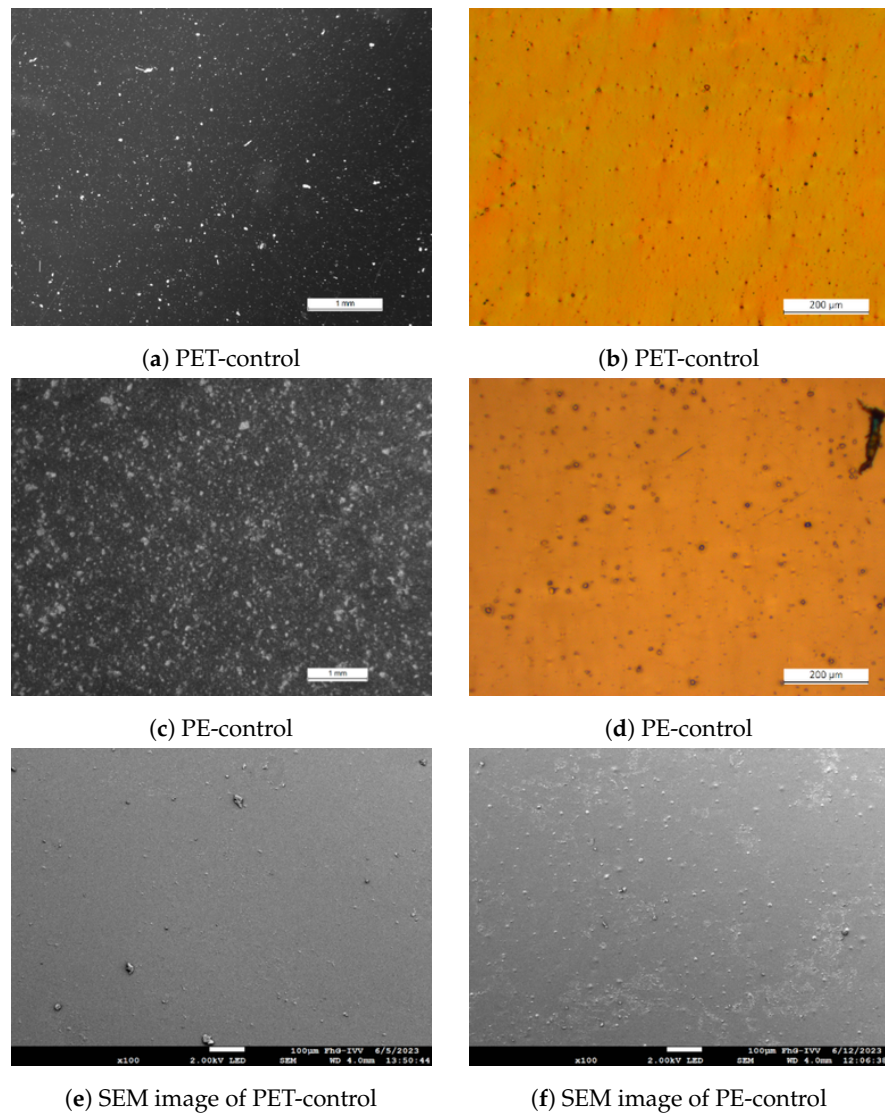


Figure A1. Stereo microscope, DIC microscope, and SEM images of uncoated PET and PE control films.

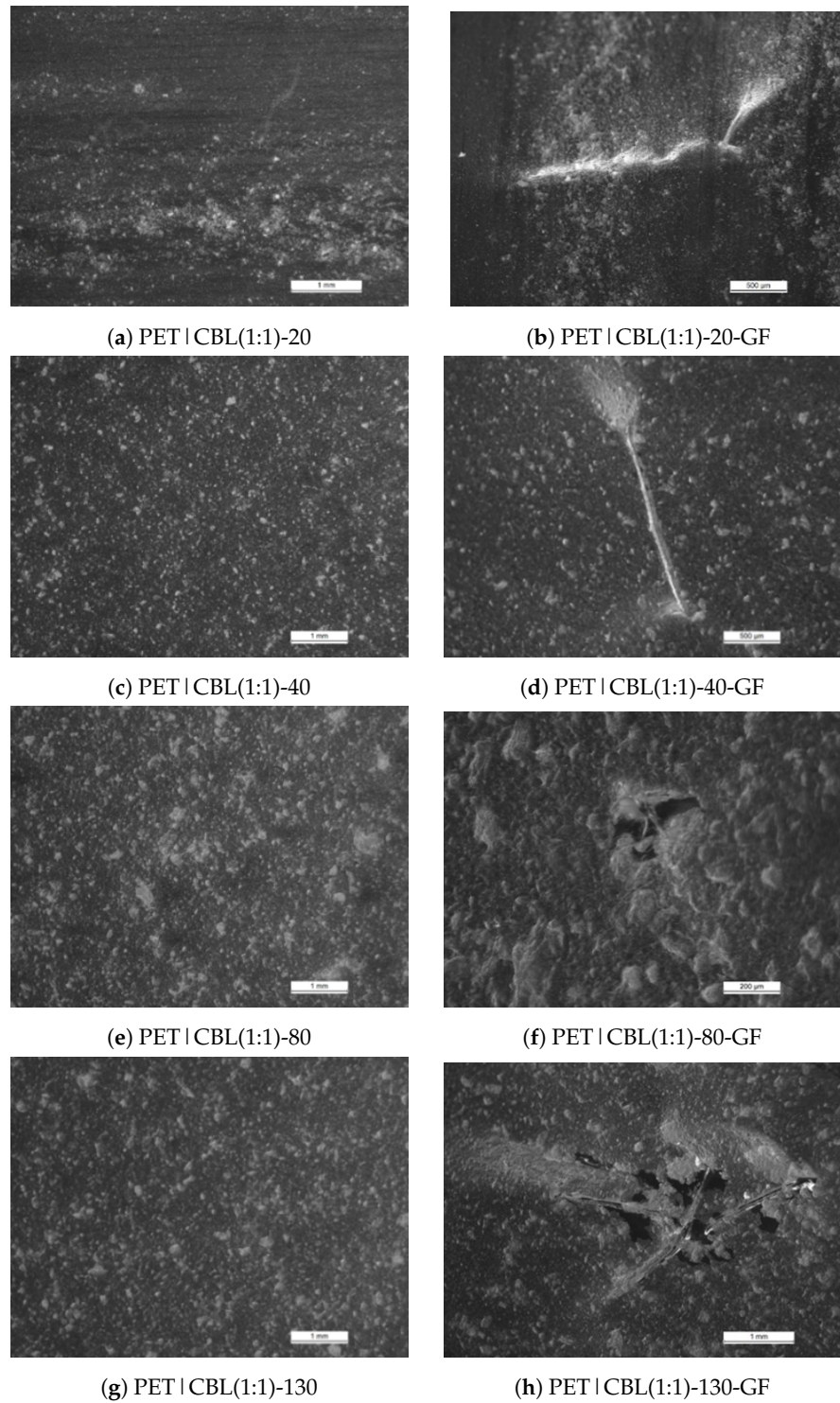
Appendix A.2. Stereo and Differential Interference Contrast Microscope Images of Coated PET

Figure A2. Stereo microscopy images of the PET films coated with different layer thicknesses of CBL(1:1) before and after Gelbo-Flex treatment.

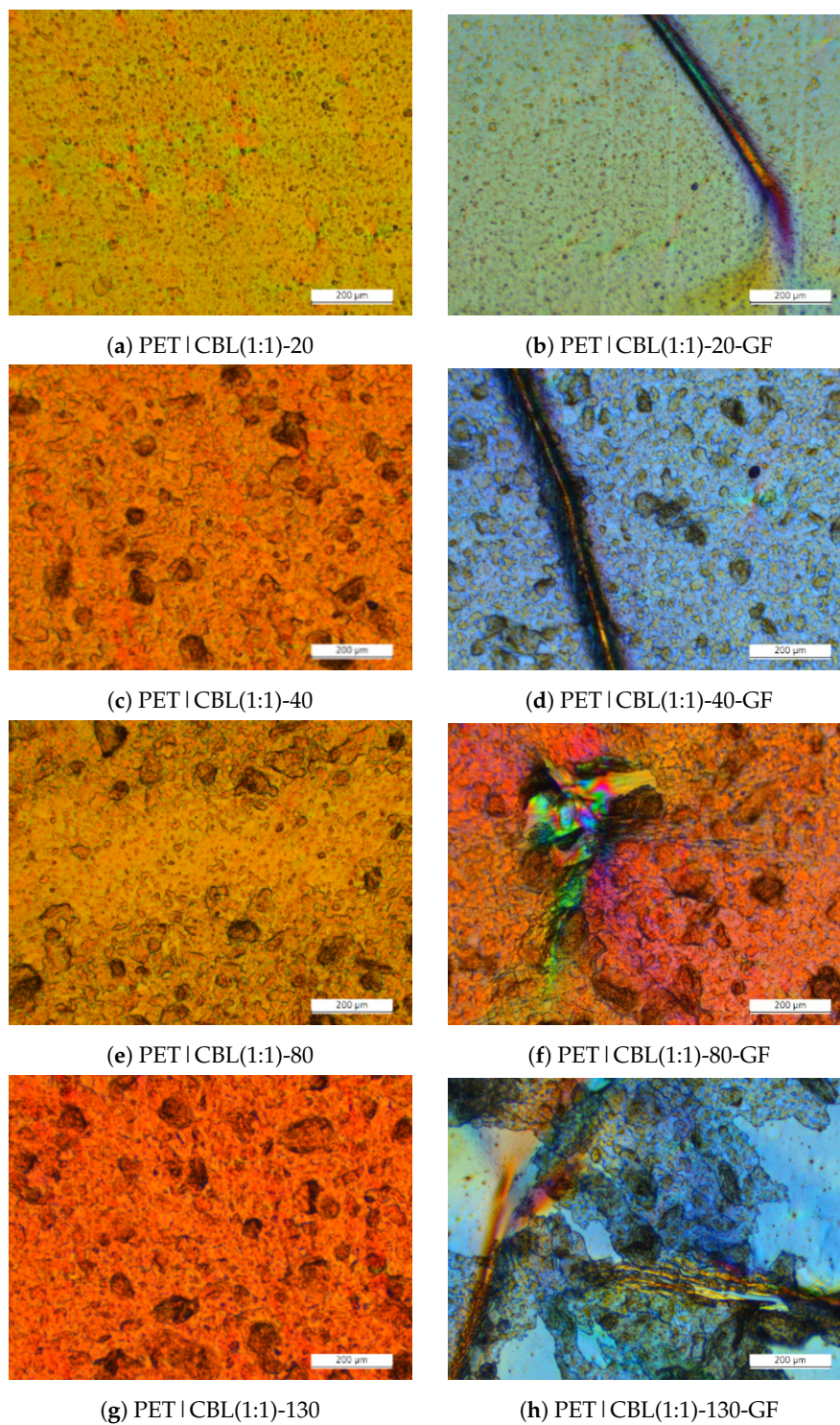


Figure A3. DIC microscopy images of the PET films coated with different layer thicknesses of CBL(1:1) before and after Gelbo-Flex treatment.

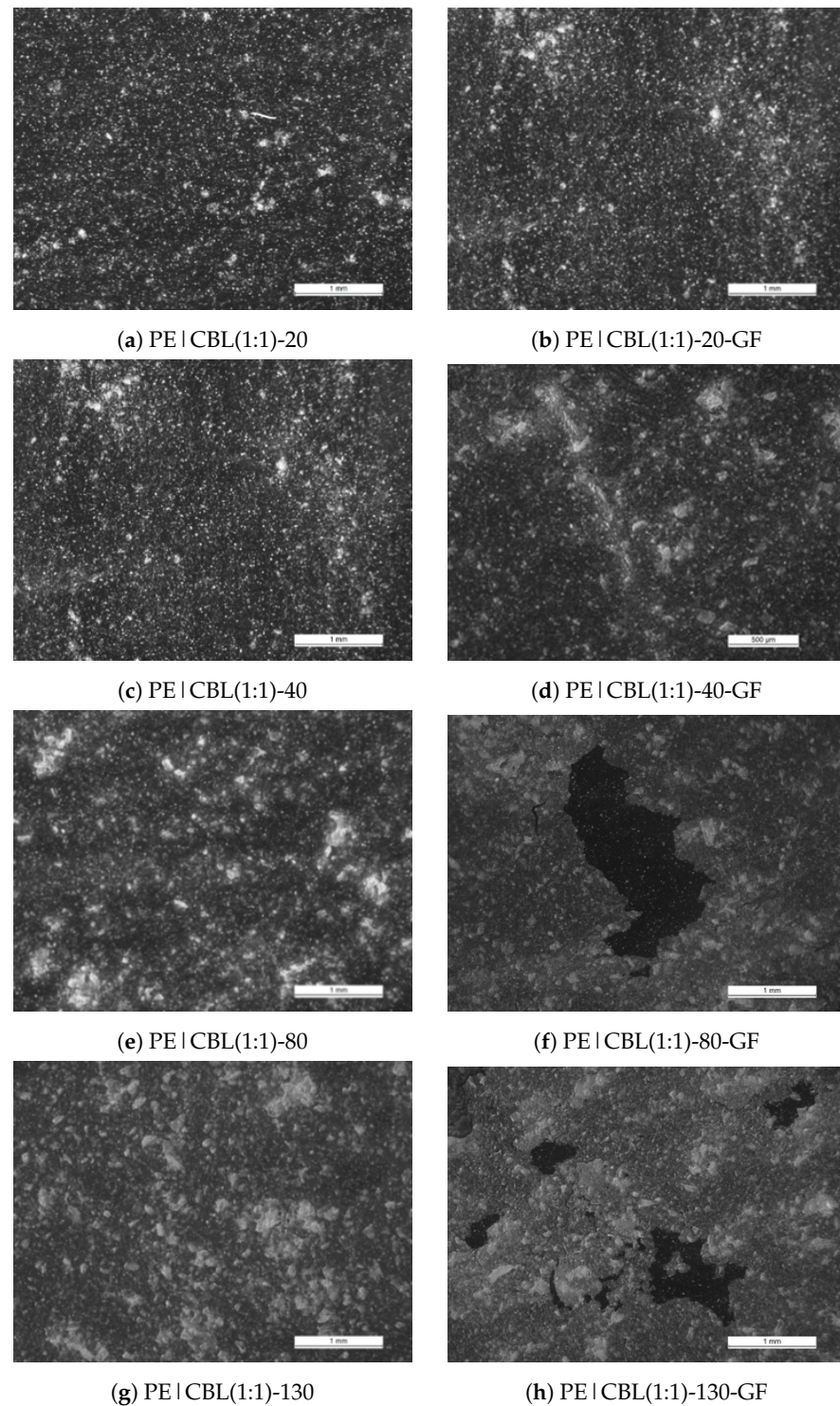
Appendix A.3. Stereo and Differential Interference Contrast Microscope Images of Coated PE

Figure A4. Stereo microscopy images of the PE films coated with different layer thicknesses of CBL(1:1) before and after Gelbo-Flex treatment.

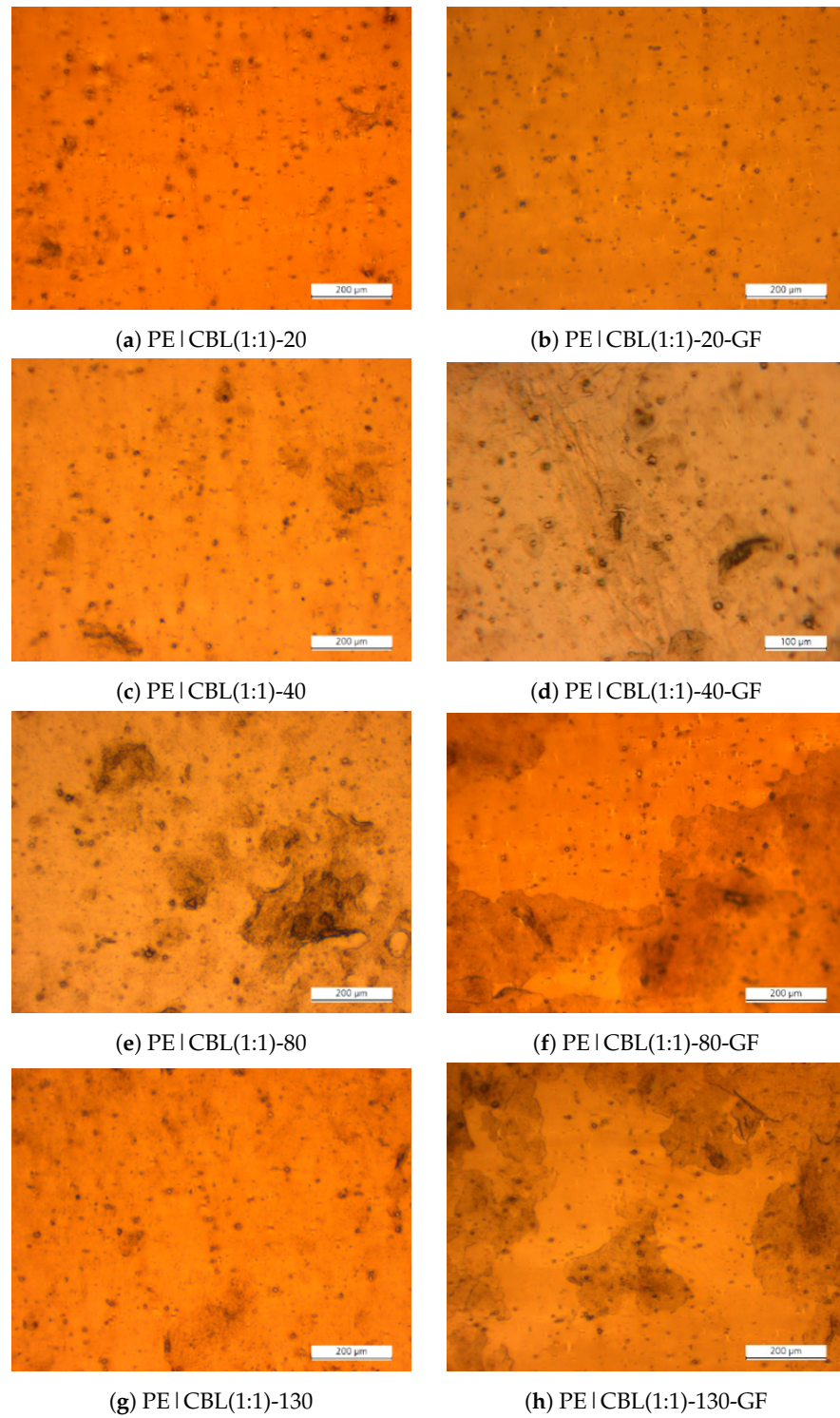


Figure A5. DIC microscopy images of the PE films coated with different layer thicknesses of CBL(1:1) before and after Gelbo-Flex treatment.

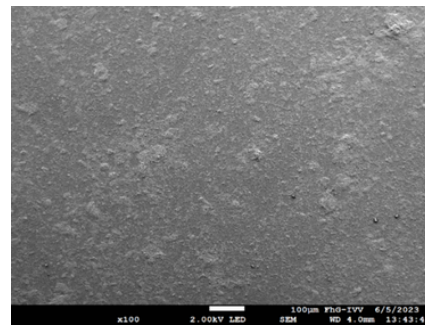
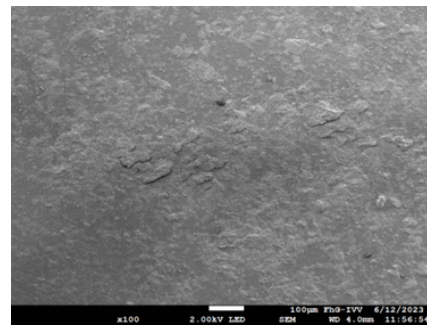
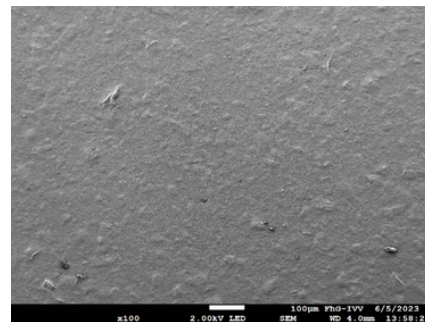
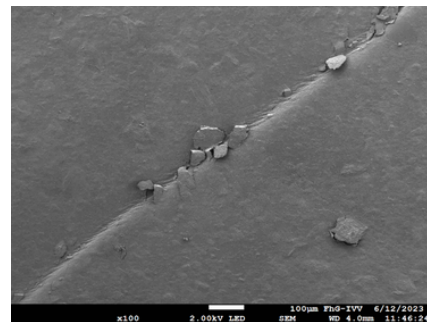
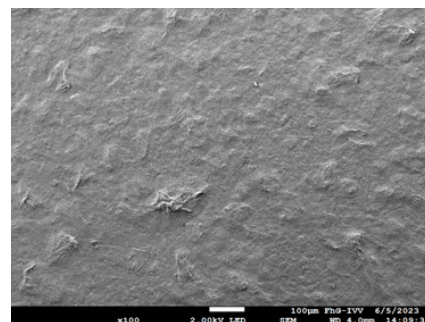
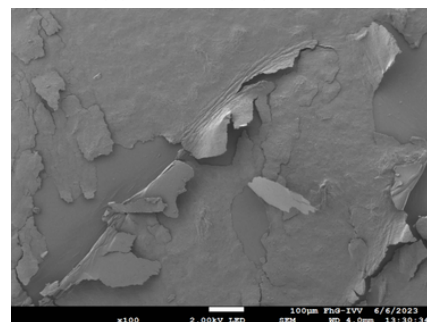
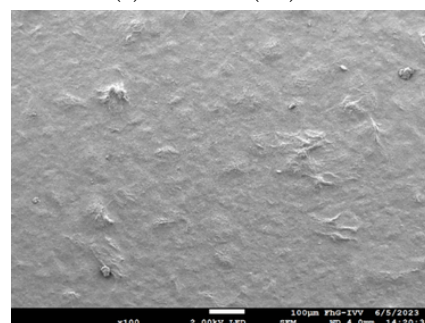
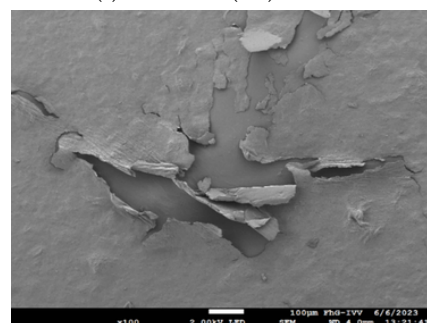
Appendix A.4. SEM Images of the Coated PET and PE Control Films**(a)** PET | CBL(1:1)-20**(b)** PET | CBL(1:1)-20-GF**(c)** PET | CBL(1:1)-40**(d)** PE | CBL(1:1)-40-GF**(e)** PET | CBL(1:1)-80**(f)** PET | CBL(1:1)-80-GF**(g)** PET | CBL(1:1)-130**(h)** PET | CBL(1:1)-130-GF

Figure A6. SEM images of the PET films coated with different layer thicknesses of CBL(1:1) before and after Gelbo-Flex treatment.

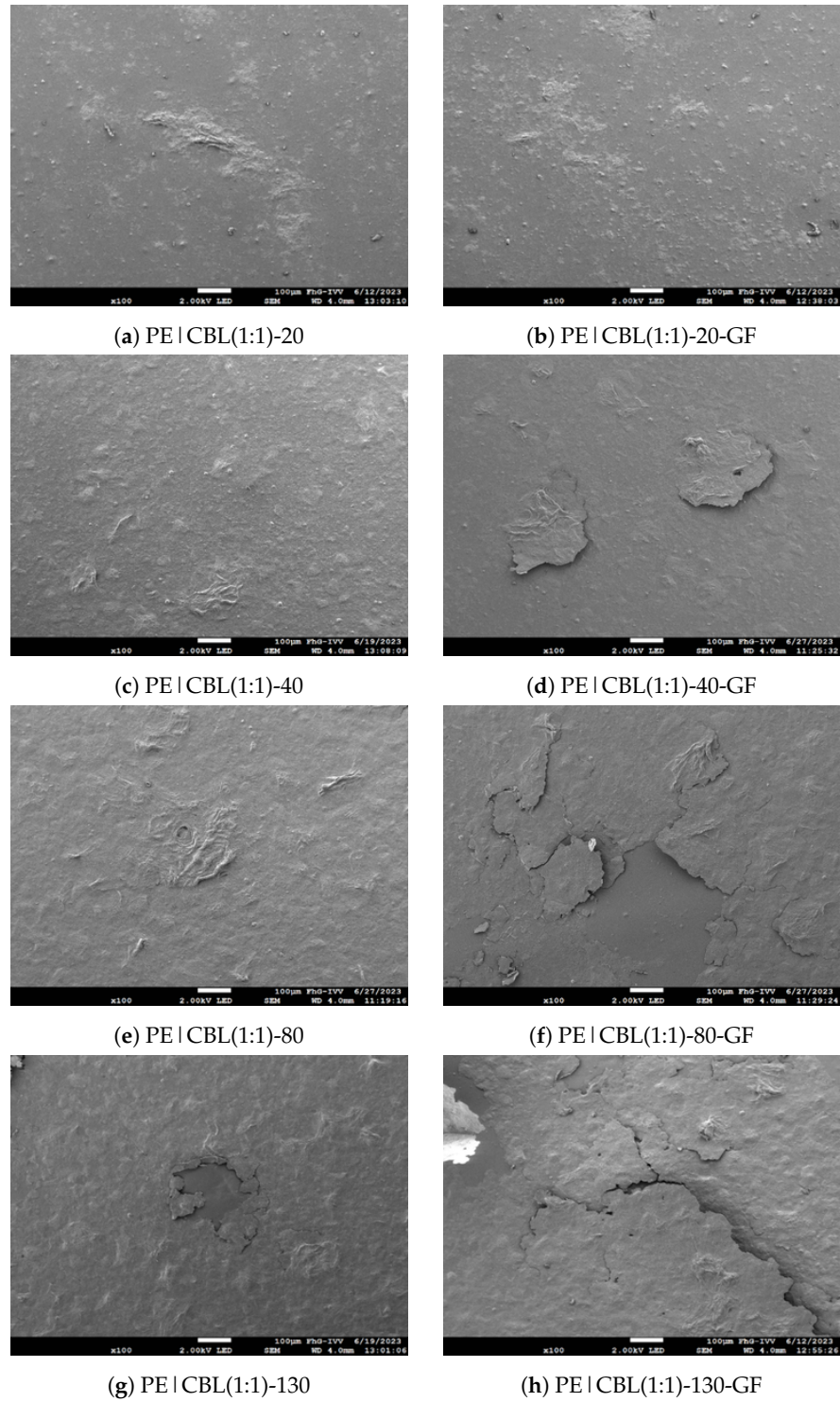


Figure A7. SEM images of the PE films coated with different layer thicknesses of CBL(1:1) before and after Gelbo-Flex treatment.

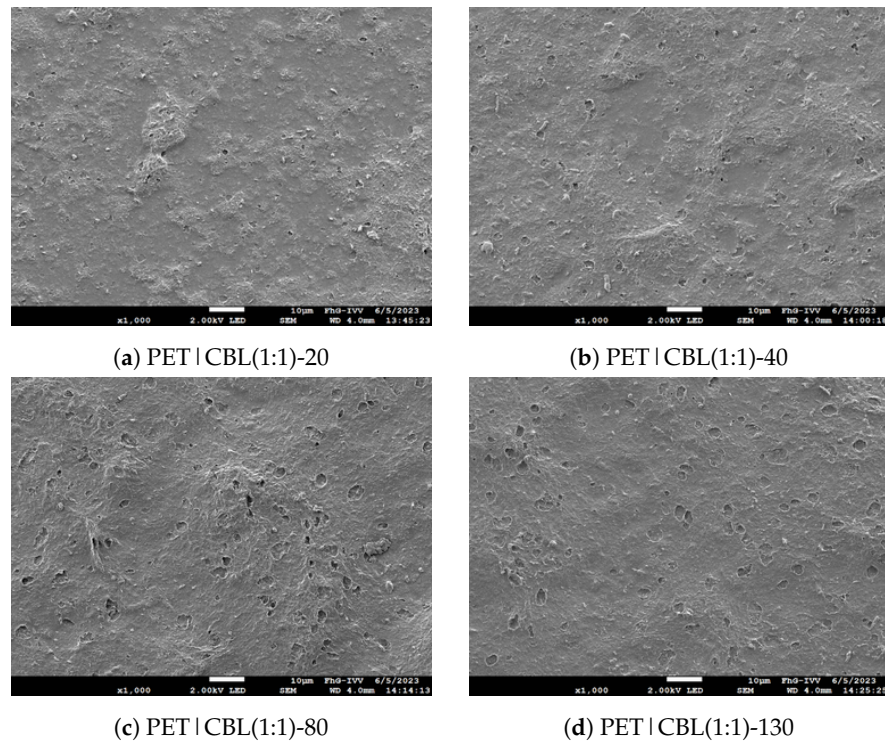


Figure A8. SEM images with a magnification of 1000 of the PET film coated with CBL(1:1) for different layer thicknesses.

Appendix A.5. Helium Permeability Coefficients of Coating Layers

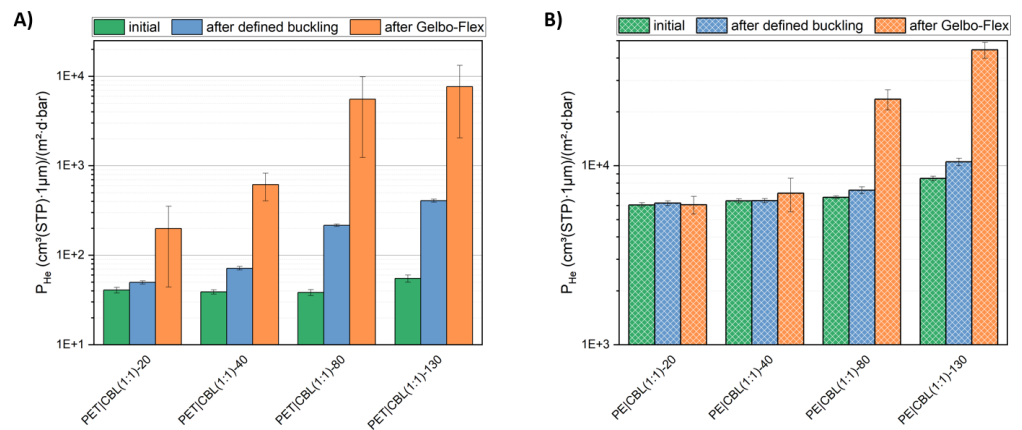


Figure A9. Helium permeability coefficients for the coating layers on PET (A) and PE (B) calculated with the values for the helium permeance (Figure 5) and the coating layer thicknesses (Table 2).

Appendix B. Effect of Formulation

Appendix B.1. Stereo and Differential Interference Contrast Microscope Images of Coated PET

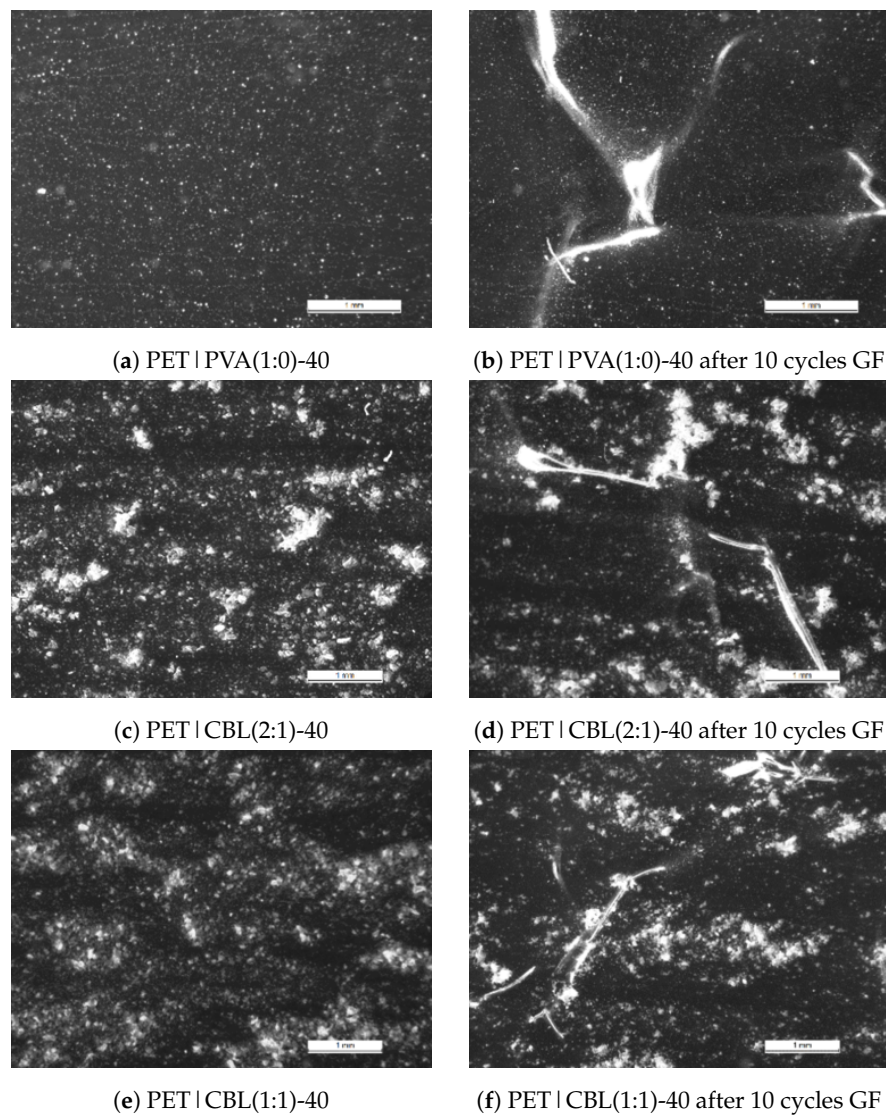


Figure A10. Stereo microscopy images of the PET films coated with lacquers with different formulations before and after Gelbo-Flex treatment.

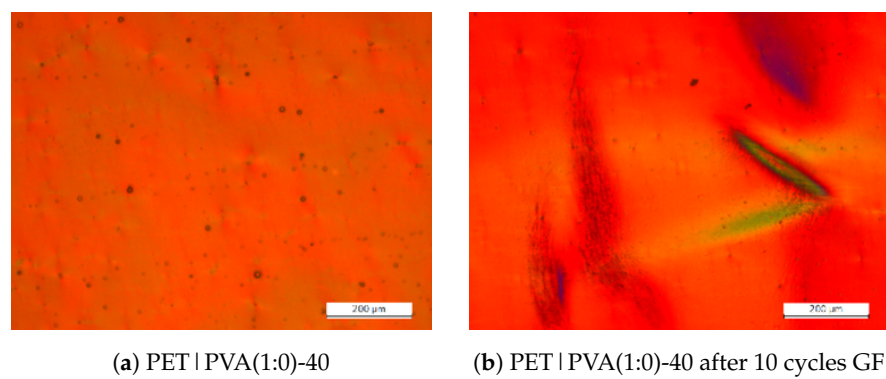


Figure A11. *Cont.*

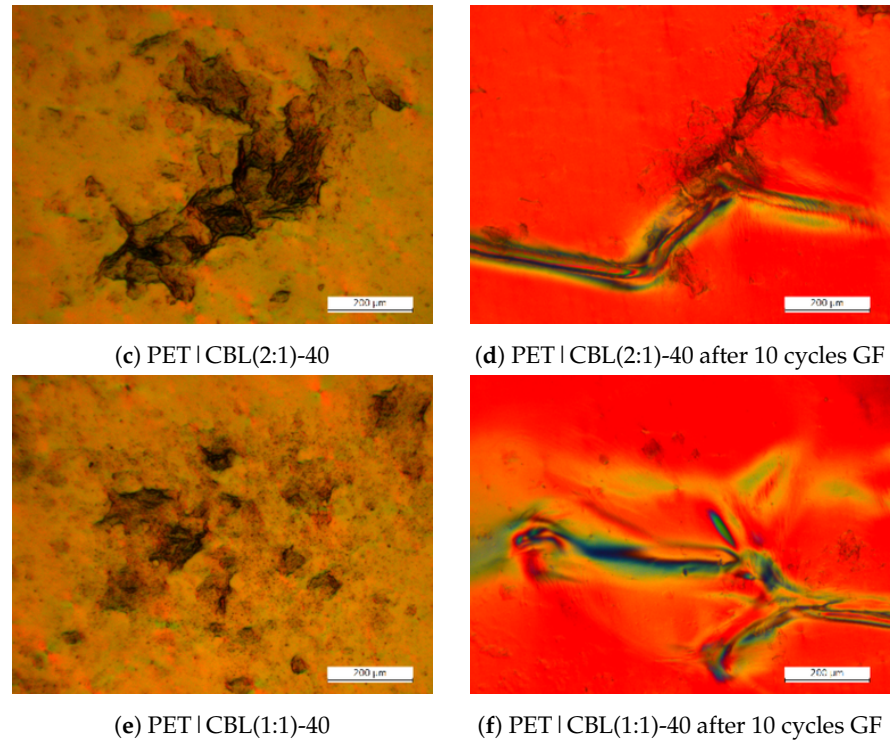


Figure A11. DIC microscopy images of the PET films coated with lacquers with different formulations before and after Gelbo-Flex treatment.

Appendix B.2. Stereo and Differential Interference Contrast Microscope Images of Coated PE

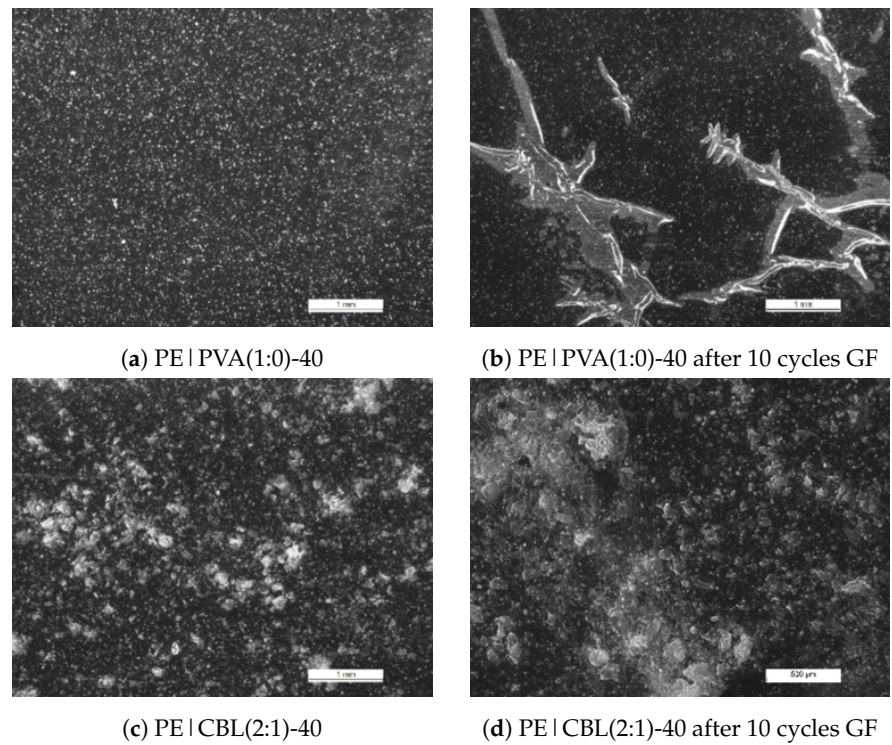


Figure A12. *Cont.*

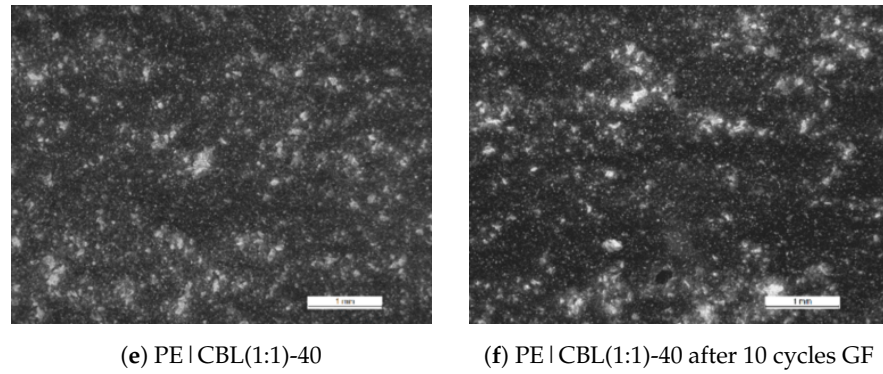


Figure A12. Stereo microscopy images of the PE films coated with lacquers with different formulations before and after Gelbo-Flex treatment.

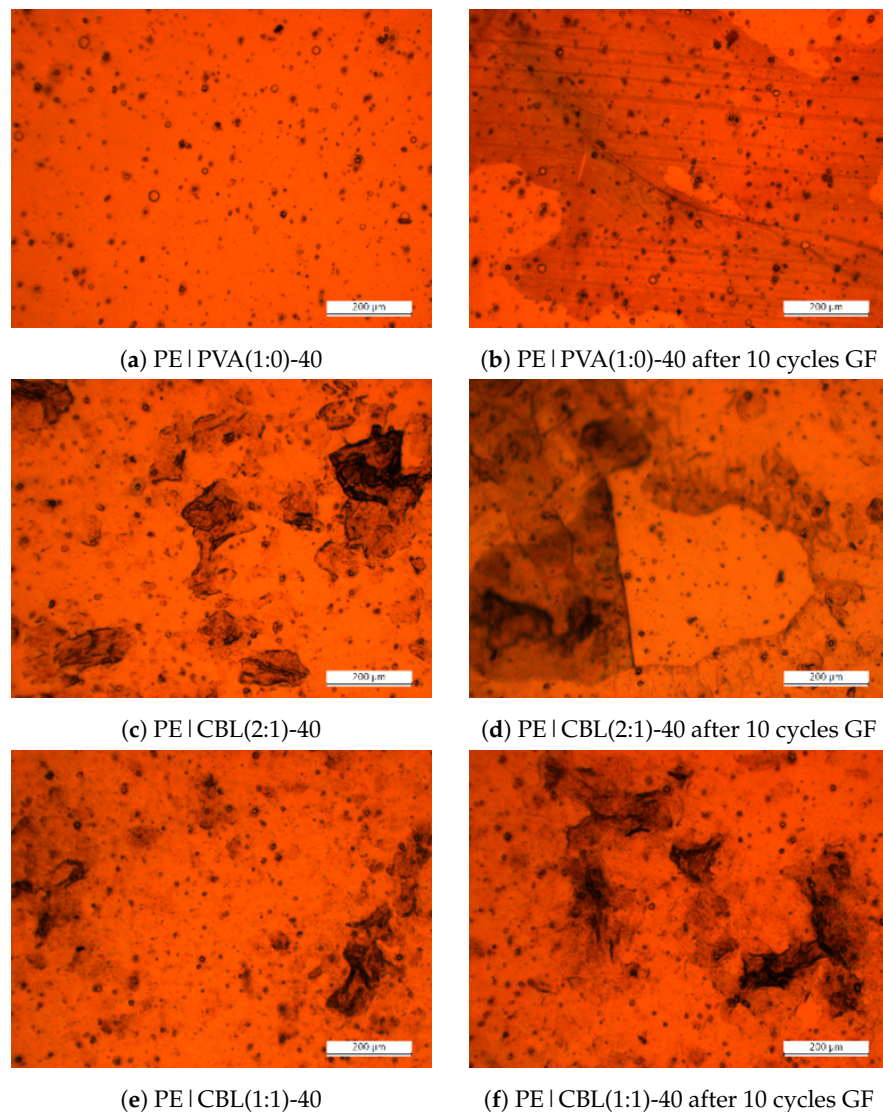


Figure A13. DIC microscopy images of the PE films coated with lacquers with different formulations before and after Gelbo-Flex treatment.

Appendix B.3. SEM Images of the Coated PET and PE Control Films

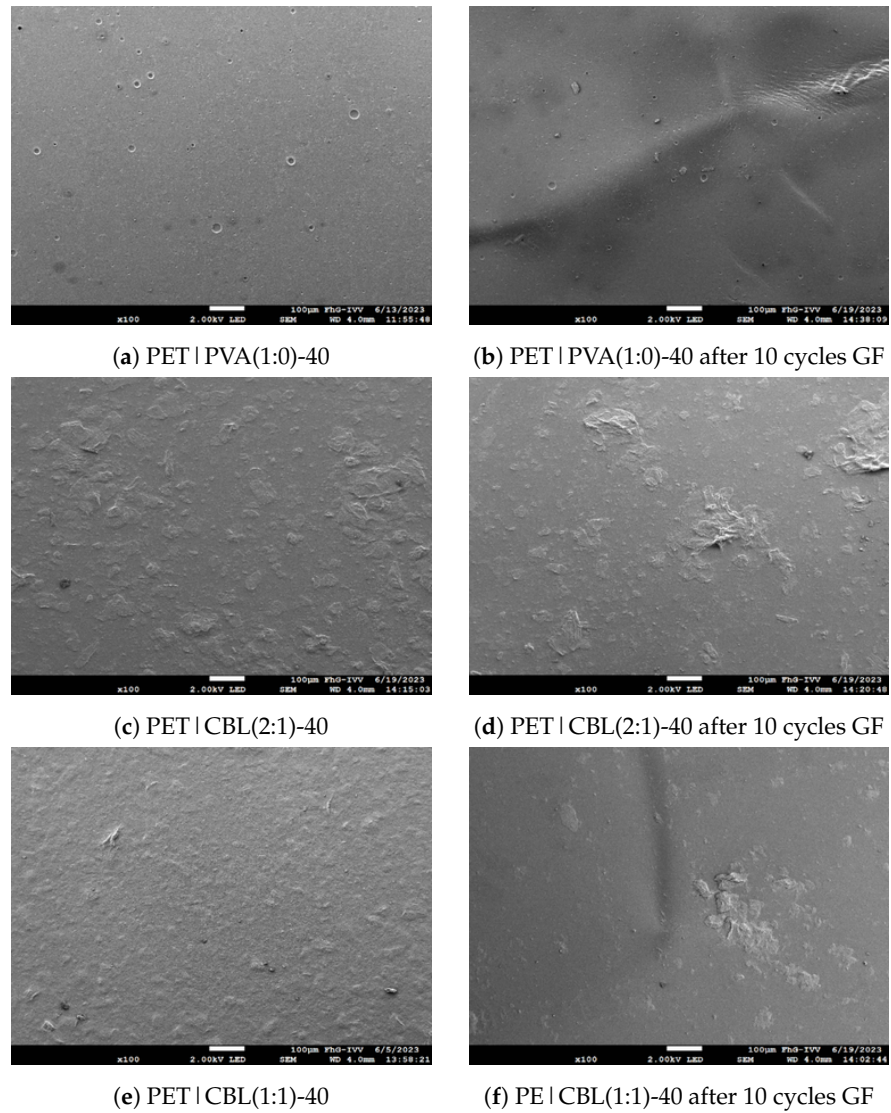


Figure A14. SEM images of the PET films coated with lacquers with different formulations before and after Gelbo-Flex treatment.

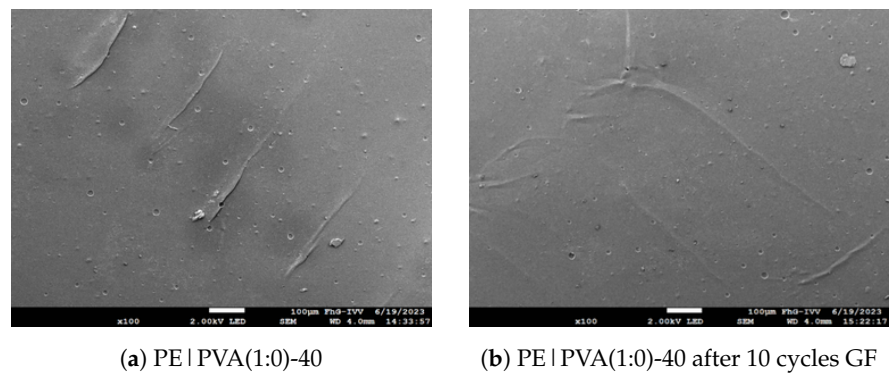


Figure A15. Cont.

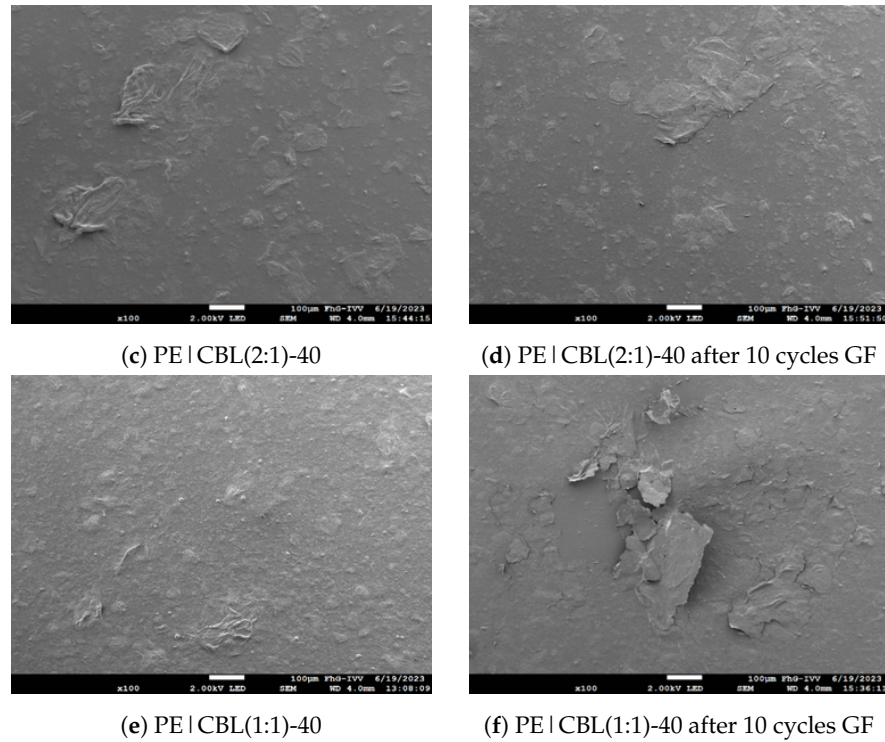


Figure A15. SEM images of the PE films coated with lacquers with different formulations before and after Gelbo-Flex treatment.

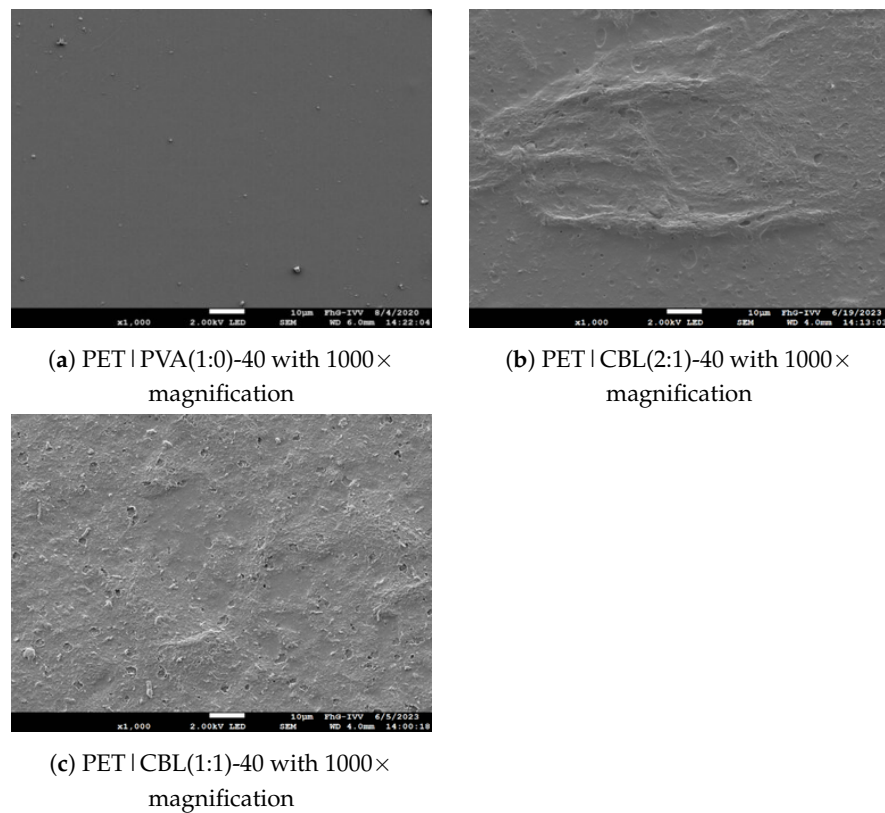


Figure A16. SEM images with a magnification of 1000 of the PET film coated with lacquers with different formulations.

Appendix B.4. Helium Permeability Coefficients of Coating Layers

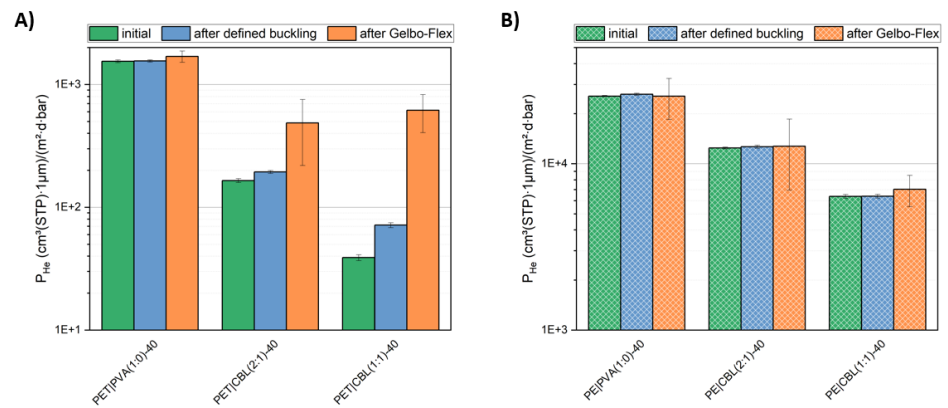


Figure A17. Helium permeability coefficients for the coating layers on PET (A) and PE (B) calculated with the values for the helium permeance (Figure 8) and the coating layer thicknesses (Table 3).

Appendix B.5. DIC Microscopy Images of Ink Test

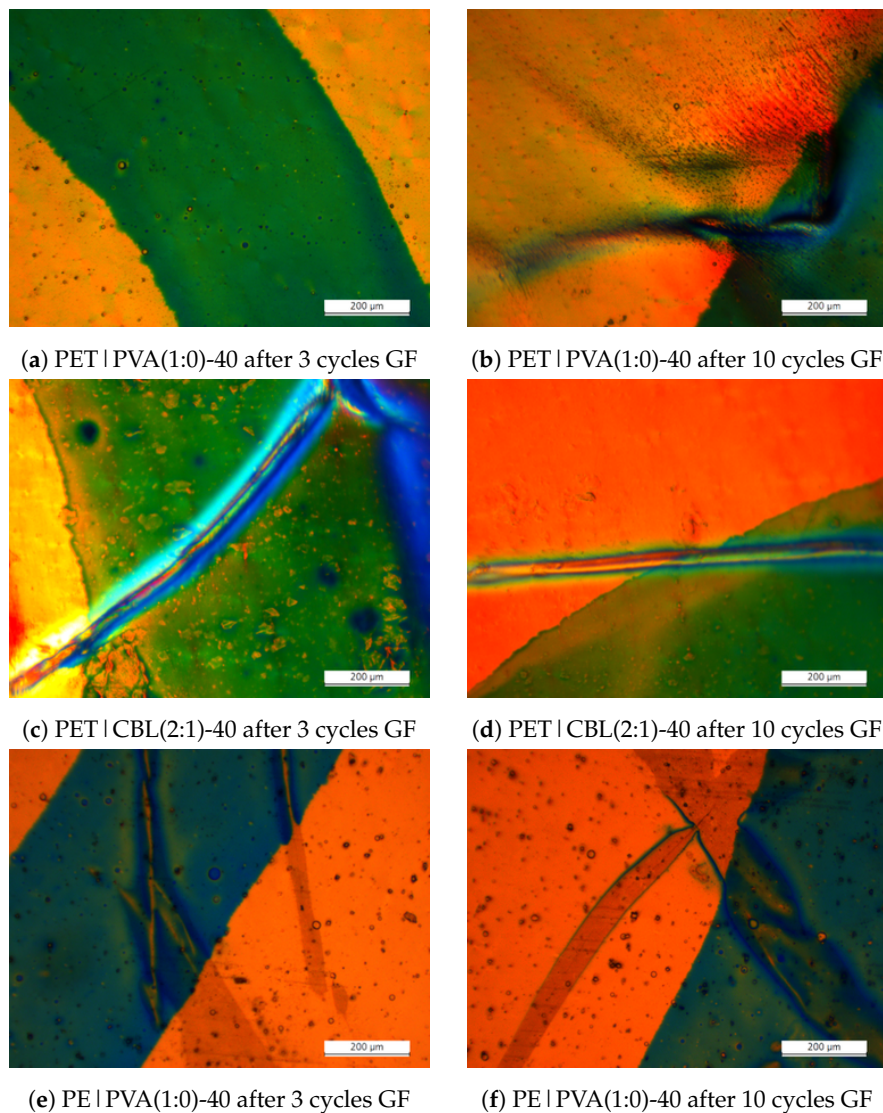


Figure A18. Cont.

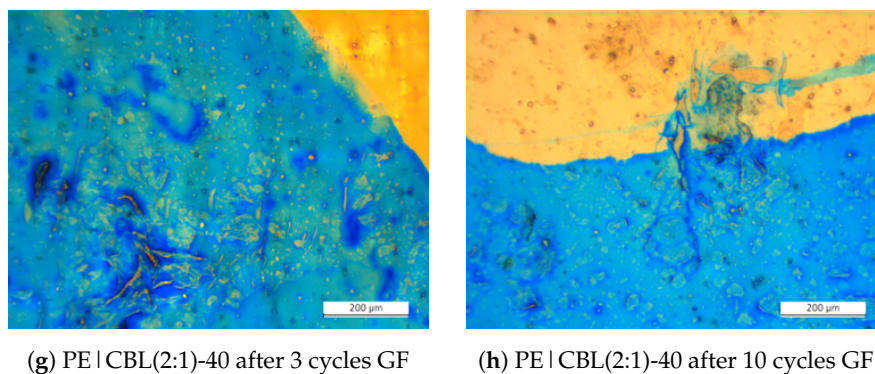


Figure A18. DIC microscope images of PET and PE coated with PVA(1:0) and CBL(2:1) after 3 and 10 cycles GF and marked with ink, respectively.

References

- Spada, A.; Conte, A.; Del Nobile, M.A. The influence of shelf life on food waste: A model-based approach by empirical market evidence. *J. Clean. Prod.* **2018**, *172*, 3410–3414. [[CrossRef](#)]
- John, J.M.; Jinap, S.; Hanani, Z.A.N.; Nor-Khaizura, M.A.R.; Samsudin, N.I.P. The effects of different packaging materials, temperatures and water activities to control aflatoxin B1 production by *Aspergillus flavus* and *A. parasiticus* in stored peanuts. *J. Food Sci. Technol.* **2019**, *56*, 3145–3150. [[CrossRef](#)] [[PubMed](#)]
- Hellwig, M. The Chemistry of Protein Oxidation in Food. *Angew. Chem. Int. Ed.* **2019**, *58*, 16742–16763. [[CrossRef](#)] [[PubMed](#)]
- Pasquier, E.; Mattos, B.D.; Koivula, H.; Khakalo, A.; Belgacem, M.N.; Rojas, O.J.; Bras, J. Multilayers of Renewable Nanostructured Materials with High Oxygen and Water Vapor Barriers for Food Packaging. *ACS Appl. Mater. Interfaces* **2022**, *14*, 30236–30245. [[CrossRef](#)] [[PubMed](#)]
- Statista Research Department. Global Market Volume of Polyethylene 2015–2030. 2023. Available online: <https://www.statista.com/statistics/1245162/polyethylene-market-volume-worldwide/> (accessed on 17 October 2024).
- Statista Research Department. Annual Production of Plastics Worldwide from 1950 to 2021. 2023. Available online: <https://www.statista.com/statistics/282732/global-production-of-plastics-since-1950/#:%E2%88%BC:text=Global%20plastics%20production%20was%20estimated,in%20production%20year%20after%20year> (accessed on 17 October 2024).
- Nisticò, R. Polyethylene terephthalate (PET) in the packaging industry. *Polym. Test.* **2020**, *90*, 106707. [[CrossRef](#)]
- Gomes, T.S.; Visconte, L.L.Y.; Pacheco, E.B.A.V. Life Cycle Assessment of Polyethylene Terephthalate Packaging: An Overview. *J. Polym. Environ.* **2019**, *27*, 533–548. [[CrossRef](#)]
- Tamburini, E.; Costa, S.; Summa, D.; Battistella, L.; Fano, E.A.; Castaldelli, G. Plastic (PET) vs bioplastic (PLA) or refillable aluminium bottles—What is the most sustainable choice for drinking water? A life-cycle (LCA) analysis. *Environ. Res.* **2021**, *196*, 110974. [[CrossRef](#)]
- Novák, I.; Popelka, A.; Špitalský, Z.; Krupa, I.; Tavman, S. Polyolefin in Packaging and Food Industry. In *Polyolefin Compounds 578 and Materials: Fundamentals and Industrial Applications*; Springer International Publishing: Cham, Switzerland, 2016; pp. 181–199. [[CrossRef](#)]
- Gerassimidou, S.; Geueke, B.; Groh, K.J.; Muncke, J.; Hahladakis, J.N.; Martin, O.V.; Iacovidou, E. Unpacking the complexity of the polyethylene food contact articles value chain: A chemicals perspective. *J. Hazard. Mater.* **2023**, *454*, 131422. [[CrossRef](#)]
- Eriksen, M.; Christiansen, J.; Daugaard, A.; Astrup, T. Closing the loop for PET, PE and PP waste from households: Influence of material properties and product design for plastic recycling. *Waste Manag.* **2019**, *96*, 75–85. [[CrossRef](#)]
- Swetha, T.A.; Bora, A.; Mohanrasu, K.; Balaji, P.; Raja, R.; Ponnuchamy, K.; Muthusamy, G.; Arun, A. A comprehensive review on polylactic acid (PLA) – Synthesis, processing and application in food packaging. *Int. J. Biol. Macromol.* **2023**, *234*, 123715. [[CrossRef](#)]
- Aznar, M.; Ubeda, S.; Dreolin, N.; Nerín, C. Determination of non-volatile components of a biodegradable food packaging material based on polyester and polylactic acid (PLA) and its migration to food simulants. *J. Chromatogr.* **2019**, *1583*, 1–8. [[CrossRef](#)] [[PubMed](#)]
- Mokwena, K.K.; Tang, J. Ethylene Vinyl Alcohol: A Review of Barrier Properties for Packaging Shelf Stable Foods. *Crit. Rev. Food Sci. Nutr.* **2012**, *52*, 640–650. [[CrossRef](#)] [[PubMed](#)]
- Andrade, J.; González-Martínez, C.; Chiralt, A. Antimicrobial PLA-PVA multilayer films containing phenolic compounds. *Food Chem.* **2022**, *375*, 131861. [[CrossRef](#)]
- Moreira, B.R.; Pereira-Júnior, M.A.; Fernandes, K.F.; Batista, K.A. An ecofriendly edible coating using cashew gum polysaccharide and polyvinyl alcohol. *Food Biosci.* **2020**, *37*, 100722. [[CrossRef](#)]
- Razmjoo, F.; Sadeghi, E.; Rouhi, M.; Mohammadi, R.; Noroozi, R.; Safajoo, S. Polyvinyl alcohol—Zedo gum edible film: Physical, mechanical and thermal properties. *J. Appl. Polym. Sci.* **2021**, *138*, 49875. [[CrossRef](#)]
- Kim, S.; Chang, Y. Anti-Salmonella polyvinyl alcohol coating containing a virulent phage PBSE191 and its application on chicken eggshell. *Food Res. Int.* **2022**, *162*, 111971. [[CrossRef](#)]

20. Settler-Ramírez, L.; López-Carballo, G.; Gavara, R.; Hernández-Muñoz, P. PVOH/protein blend films embedded with lactic acid bacteria and their antilisterial activity in pasteurized milk. *Int. J. Food Microbiol.* **2020**, *322*, 108545. [[CrossRef](#)]
21. Grunlan, J.C.; Grigorian, A.; Hamilton, C.B.; Mehrabi, A.R. Effect of clay concentration on the oxygen permeability and optical properties of a modified poly(vinyl alcohol). *J. Appl. Polym. Sci.* **2004**, *93*, 1102–1109. [[CrossRef](#)]
22. Gaume, J.; Taviot-Gueho, C.; Cros, S.; Rivaton, A.; Thérias, S.; Gardette, J.L. Optimization of PVA clay nanocomposite for ultra-barrier multilayer encapsulation of organic solar cells. *Sol. Energy Mater. Sol. Cells* **2012**, *99*, 240–249. [[CrossRef](#)]
23. Nyflött, A.; Carlsson, G.; Järnström, L.; Lestelius, M.; Moons, E.; Wahlström, T.; Axrup, L. Influence of kaolin addition on the dynamics of oxygen mass transport in polyvinyl alcohol dispersion coatings. *Nord. Pulp Pap. Res. J.* **2015**, *30*, 385–392. [[CrossRef](#)]
24. Ben Dhieb, F.; Tabatabaei, S.H.; Mighri, F.; Aji, A. Comparison of Crosslinking Efficiency in Dip and Roll-Deposited Coatings on Their Oxygen Barrier. *ACS Omega* **2019**, *4*, 15772–15779. [[CrossRef](#)] [[PubMed](#)]
25. Schiessl, S.; Kucukpinar, E.; Cros, S.; Miesbauer, O.; Langowski, H.C.; Eisner, P. Nanocomposite Coatings Based on Polyvinyl Alcohol and Montmorillonite for High-Barrier Food Packaging. *Front. Nutr.* **2022**, *9*, 790157. [[CrossRef](#)] [[PubMed](#)]
26. Schiessl, S.; Kucukpinar, E.; Schwiddessen, R.; Langowski, H.C.; Eisner, P. Mechanisms of permeation of helium, hydrogen, oxygen, and water vapor through silicate-based composite barrier coating layers. *Surf. Coat. Technol.* **2024**, *483*, 130800. [[CrossRef](#)]
27. Lim, M.; Kwon, H.; Kim, D.; Seo, J.; Han, H.; Khan, S.B. Highly-enhanced water resistant and oxygen barrier properties of cross-linked poly(vinyl alcohol) hybrid films for packaging applications. *Prog. Org. Coat.* **2015**, *85*, 68–75. [[CrossRef](#)]
28. Müller, K.; Scheuerer, Z.; Florian, V.; Skutschik, T.; Sänglerlaub, S. Comparison of test methods for oxygen permeability: Optical method versus carrier gas method. *Polym. Test.* **2017**, *63*, 126–132. [[CrossRef](#)]
29. Hare, B.A.; Moyse, A.; Sue, H.J. Analysis of scratch-induced damages in multi-layer packaging film systems. *J. Mater. Sci.* **2012**, *47*, 1389–1398. [[CrossRef](#)]
30. DIN ISO 8296; DIN Deutsches Institut für Normung e.V. Plastics-Film and Sheeting-Determination of Wetting Tension. ISO: London, UK, 2008.
31. Bradley, E.; Castle, L.; Dines, T.; Fitzgerald, A.; Gonzalez Tunon, P.; Jickells, S.; Johns, S.; Layfield, E.; Mountfort, K.; Onoh, H.; et al. Test method for measuring non-visible set-off from inks and lacquers on the food-contact surface of printed packaging materials. *Food Addit. Contam.* **2005**, *22*, 490–502. [[CrossRef](#)]
32. DIN 53380-2; DIN Deutsches Institut für Normung e.V. Testing of Plastics—Determination of Gas Transmission Rate—Part 2: Manometric Method for Testing of Plastic Films. ISO: London, UK, 2006.
33. Mansuri, A.; Kumar, A. Introduction to Stereo Microscope. In *Forensic Microscopy: Truth Under the Lenses*; CRC: Boca Raton, FL, USA, 2022. [[CrossRef](#)]
34. Simon, J.M.; Comastri, S.A. The compound microscope: Optical tube length or parfocalization? *Eur. J. Phys.* **2005**, *26*, 1101. [[CrossRef](#)]
35. ASTM F392/F392M-21; Standard Practice for Conditioning Flexible Barrier Materials for Flex Durability. ASTM International: West Conshohocken, PA, USA, 2023.
36. DIN EN ISO 527-3; DIN Deutsches Institut für Normung e.V. Plastics—Determination of Tensile Properties—Part 3: TEST Conditions for Films and Sheets (ISO 527-3:2018). ISO: London, UK 2006.
37. Barrer, R.M. *Diffusion in and Through Solids*; University Press: Oxford, UK, 1941.
38. McMaster, R.C. *Nondestructive Testing Handbook*, 2nd ed.; Amer Society for Nondestructive: Columbus, OH, USA, 1982; Volume 2.
39. ISO 3452-1:2021; Non-Destructive Testing. Penetrant Testing—Part 1: General Principles. ISO: London, UK, 2021.
40. Dobrowszky, K.; Ronkay, F. Effects of Phase Inversion on Molding Shrinkage, Mechanical, and Burning Properties of Injection-molded PET/HDPE and PS/HDPE Polymer Blends. *Polym.-Plast. Technol. Eng.* **2017**, *56*, 1147–1157. [[CrossRef](#)]
41. Li, F.; Biagioni, P.; Bollani, M.; Maccagnan, A.; Piergiovanni, L. Multi-functional coating of cellulose nanocrystals for flexible packaging applications. *Cellulose* **2013**, *20*, 2491–2504. [[CrossRef](#)]
42. Aidun, C.K.; Triantafillopoulos, N.G. High-Speed Blade Coating. In *Liquid Film Coating: Scientific Principles and Their Technological Implications*; Springer: Dordrecht, The Netherlands, 1997; pp. 637–672. [[CrossRef](#)]
43. Yan, X.; Yang, L.; An, Y.; Jin, W.; Li, Y.; Li, B. Surface roughness and hydrophilicity enhancement of polyolefin-based membranes by three kinds of plasma methods. *Surf. Interface Anal.* **2015**, *47*, 545–553. [[CrossRef](#)]
44. Oliveira, K.M.C.; Consani, S.; Gonçalves, L.S.; Brandt, W.C.; Ccahuana-Vásquez, R.A. Photoelastic evaluation of the effect of composite formulation on polymerization shrinkage stress. *Braz. Oral Res.* **2012**, *26*, 202–208. [[CrossRef](#)] [[PubMed](#)]
45. Faisant, J.; Ait-Kadi, A.; Bousmina, M.; Desche^nes, L. Morphology, thermomechanical and barrier properties of polypropylene-ethylene vinyl alcohol blends. *Polymer* **1998**, *39*, 533–545. [[CrossRef](#)]
46. Felts, J.T. Transparent Barrier Coatings Update: Flexible Substrates. *J. Plast. Film. Sheeting* **1993**, *9*, 139–158. [[CrossRef](#)]
47. Aydemir, C.; Altay, B.N.; Akyol, M. Surface analysis of polymer films for wettability and ink adhesion. *Color Res. Appl.* **2021**, *46*, 489–499. [[CrossRef](#)]
48. Azar, G.T.P.; Yelkarasi, C.; Ürgen, M. The role of droplets on the cavitation erosion damage of TiN coatings produced with cathodic arc physical vapor deposition. *Surf. Coat. Technol.* **2017**, *322*, 211–217. [[CrossRef](#)]
49. Karimi, A.; Wan Daud, W.M.A. Harmless hydrogels based on PVA/Na⁺-MMT nanocomposites for biomedical applications: Fabrication and characterization. *Polym. Compos.* **2017**, *38*, 1135–1143. [[CrossRef](#)]
50. Yu, Y.H.; Lin, C.Y.; Yeh, J.M.; Lin, W.H. Preparation and properties of poly(vinyl alcohol)-clay nanocomposite materials. *Polymer* **2003**, *44*, 3553–3560. [[CrossRef](#)]

51. Schiessl, S.; Kucukpinar, E.; Rivollier, N.; Langowski, H.C.; Eisner, P. A Comparative Study on the Roll-to-Roll Processing of a Silicate—Polyvinyl Alcohol Composite Barrier Lacquer Using Slot-Die and Reverse Gravure Coating Techniques. *Polymers* **2023**, *15*, 2761. [[CrossRef](#)]
52. Singh, R. Penetrant Testing. In *Applied Welding Engineering: Processes, Codes, and Standards*; Butterworth-Heinemann: Oxford, UK, 2020; pp. 283–291.

Disclaimer/Publisher’s Note: The statements, opinions and data contained in all publications are solely those of the individual author(s) and contributor(s) and not of MDPI and/or the editor(s). MDPI and/or the editor(s) disclaim responsibility for any injury to people or property resulting from any ideas, methods, instructions or products referred to in the content.